Author Manuscript

Author Manuscript

Author Manuscript

Author Manuscript

HHS Public Access

Author manuscript

Neuron. Author manuscript; available in PMC 2019 April 18.

Published in final edited form as:

Neuron. 2018 April 18; 98(2): 335–349.e7. doi:10.1016/j.neuron.2018.03.011.

RIM C_2B domains target presynaptic active zone functions to PIP_2-containing membranes

Arthur PH de Jong[1], **Carlos M Roggero**[2], **Meng-Ru Ho**[2,3], **Man Yan Wong**[1], **Chad A. Brautigam**[4], **Josep Rizo**[2], and **Pascal S Kaeser**[1,#]

[1]Department of Neurobiology, Harvard Medical School, Boston MA USA 02115

[2]Departments of Biophysics, Biochemistry and Pharmacology, University of Texas Southwestern Medical Center, Dallas TX USA 75390

[3]Institute of Biological Chemistry, Academia Sinica, Taipei, Taiwan

[4]Departments of Biophysics and Microbiology, University of Texas Southwestern Medical Center, Dallas TX USA 75390

Summary

Rapid and efficient synaptic vesicle fusion requires a pool of primed vesicles, the nearby tethering of Ca^{2+} channels, and the presence of the phospholipid PIP_2 in the target membrane. While the presynaptic active zone mediates the first two requirements, it is unclear how fusion is targeted to membranes with high PIP_2 content. Here, we find that the C_2B domain of the active zone scaffold RIM is critical for action potential-triggered fusion. Remarkably, the known RIM functions in vesicle priming and Ca^{2+}-influx do not require RIM C_2B domains. Instead, biophysical experiments reveal that RIM C_2 domains, which lack Ca^{2+} binding, specifically bind to PIP_2. Mutational analyses establish that PIP_2 binding to RIM C_2B and its tethering to the other RIM domains are crucial for efficient exocytosis. We propose that RIM C_2B domains are constitutive PIP_2-binding modules that couple mechanisms for vesicle priming and Ca^{2+} channel tethering to PIP_2-containing target membranes.

eTOC Blurb (in Brief)

De Jong et. al. demonstrate that the RIM C_2B domain is important for neurotransmitter release. RIM C_2B binds to the phospholipid PIP_2, and this interaction directs synaptic vesicle priming and Ca^{2+} influx to the PIP_2-containing plasma membrane for efficient exocytosis.

[#]corresponding author and lead contact: kaeser@hms.harvard.edu.

Declaration of Interests

The authors have no conflicts of interest to declare.

Author Contributions

Conceptualization, A.d.J., J.R. and P.S.K.; Methodology, A.d.J., J.R. and P.S.K.; Formal Analysis, A.d.J., M.H., C.R., J.R. and P.S.K.; Investigation, A.d.J., M.H., C.R., M.Y.W. and C.B.; Writing-Original Draft, A.d.J. and P.S.K..; Supervision, J.R. and P.S.K.; Funding Acquisition A.d.J., J.R. and P.S.K.

Publisher's Disclaimer: This is a PDF file of an unedited manuscript that has been accepted for publication. As a service to our customers we are providing this early version of the manuscript. The manuscript will undergo copyediting, typesetting, and review of the resulting proof before it is published in its final citable form. Please note that during the production process errors may be discovered which could affect the content, and all legal disclaimers that apply to the journal pertain.

Author Manuscript Author Manuscript Author Manuscript Author Manuscript

Introduction

Information transfer between neurons is initiated by rapid fusion of synaptic vesicles in presynaptic nerve terminals. Synaptic vesicle exocytosis is restricted to the active zone, a protein complex that is tightly attached to the presynaptic membrane and that controls the fusion machinery (Südhof, 2012). The membrane fusion reaction itself is driven by a conserved molecular machinery, composed of SNARE proteins and Munc18, among others (Jahn and Fasshauer, 2012). This machinery is highly homologous to those of secretory pathways in non-neuronal cells and unicellular organisms (Wickner, 2010) that operate without active zone-like scaffolds, and fusion itself is thought to occur independent of active zone proteins (Südhof, 2013).

To ensure the spatiotemporal precision of synaptic vesicle fusion, three fundamental requirements must be met. First, vesicles must undergo maturation steps to become highly fusogenic, broadly referred to as docking and priming (Kaeser and Regehr, 2017; Südhof, 2012). Second, voltage gated Ca^{2+} channels must be anchored near fusion ready vesicles such that local Ca^{2+} levels rise and fall quickly in response to a presynaptic action potential for rapid, synchronous fusion triggering (Eggermann et al., 2012). Third, efficient fusion relies on specific lipids, in particular the presence of phosphatidylinositol 4,5-bisphosphate (PIP_2) in the target membrane (Hay et al., 1995; Milosevic et al., 2005; Di Paolo et al., 2004). The importance for PIP_2 in fusion arises from its ability to boost presynaptic Ca^{2+} entry and the Ca^{2+}-affinity of the fusion machinery (Van den Bogaart et al., 2012; Suh et al., 2010). In many secretory cells, PIP_2 is not evenly distributed across membranes, but is restricted to the plasma membrane, where it forms small clusters (Aoyagi et al., 2005; van den Bogaart et al., 2011; Laux et al., 2000). While the exact distribution of PIP_2 within a nerve terminal is not known, PIP_2 defines plasma membrane identity (Di Paolo and De Camilli, 2006) and is essential for synaptic vesicle exocytosis (Di Paolo et al., 2004). It is further often hypothesized that PIP_2 is clustered at the active zone (van den Bogaart et al., 2011; Lauwers et al., 2016). Hence, mechanisms that target the fusion machinery to PIP_2-containing membranes are necessary. While a growing body of knowledge strongly supports the notion that the active zone provides molecular mechanisms for the first two requirements, it is unclear how these active zone functions are targeted to PIP_2-containing membranes.

Active zones, which are composed of RIM, RIM-BP, ELKS, Munc13, Piccolo/Bassoon and Liprin-α, control the docking and priming of synaptic vesicles and the nearby anchoring of Ca^{2+} channels (Südhof, 2012). RIMs recruit Ca^{2+}-channels in a tripartite complex with RIM-BPs (Han et al., 2011; Hibino et al., 2002; Kaeser et al., 2011; Liu et al., 2011). This recruitment is mediated by the central RIM PDZ domain, which binds to Ca^{2+} channels, and a proline-rich PxxP motif between two C-terminal C_2 domains that binds to RIM-BPs, which in turn bind to Ca^{2+}-channels as well (Figure 1A). Via its N-terminal zinc finger domain, RIM activates and anchors Munc13 to control the number of docked and primed vesicles (Andrews-Zwilling et al., 2006; Augustin et al., 1999; Camacho et al., 2017; Deng et al., 2011; Han et al., 2011; Imig et al., 2014). Thus, RIM proteins have evolved as essential scaffolds that participate in these key active zone functions (Figure 1A).

Author Manuscript Author Manuscript Author Manuscript Author Manuscript

The two RIM C_2 domains, termed C_2A and C_2B, remain poorly understood despite being highly conserved sequences across RIM proteins (Wang and Südhof, 2003). C_2 domains are widely known as Ca^{2+} sensors (Südhof, 2013), but RIM C_2 domains cannot bind Ca^{2+} (Dai et al., 2005; Guan et al., 2007). Several interactors for RIM C_2A or C_2B have been identified in vitro. These include Liprin-α, SNAREs, Ca^{2+} channel β-subunits, and synaptotagmins (Coppola et al., 2001; Kaeser et al., 2012; Kiyonaka et al., 2007; Schoch et al., 2002), and RIM C_2B domains also dimerize (Guan et al., 2007), but the physiological relevance of these interactions at synapses remains unclear. In *C. elegans*, removal of the C_2B domain leads to a behavioral phenotype similar to RIM null mutants (Koushika et al., 2001). Together with the high conservation, this finding suggests important roles for RIM C_2B, but it is unknown if this is due to defects in expression and localization of RIM, or due to a more direct role in synaptic transmission. Notably, RIM C_2B contains a lysine-rich polybasic stretch with high homology to several other C_2 domains (Corbalan-Garcia and Gómez-Fernández, 2014). In such C_2 domains, this motif binds to PIP_2 (Bai et al., 2004; Coudevylle et al., 2008; Guerrero-Valero et al., 2009), and mutations in this motif lead to biochemical defects and impaired synaptic transmission (Van den Bogaart et al., 2012; Groffen et al., 2010; Li et al., 2006).

Given the central scaffolding role for RIM at the active zone, constitutive binding of its C_2 domains to PIP_2 could provide an attractive mechanism to target synaptic vesicle docking, priming and Ca^{2+} channel tethering to PIP_2-containing membranes. Here, we tested this hypothesis and found that both RIM C_2 domains bind PIP_2. Deleting the RIM C_2B domain or disrupting PIP_2 binding to the RIM C_2B domain strongly impaired synaptic transmission, whereas similar manipulations of the RIM C_2A domain did not have strong functional effects. Remarkably, while binding of the C_2B domain to PIP_2 was required for rescue of action potential triggered vesicle fusion, removing C_2B did not impair the known RIM functions in vesicle priming and Ca^{2+}-influx. Finally, RIM C_2B domains were inactive unless they were attached to the N-terminal RIM domains. We propose that RIM C_2B domains tether essential active zone functions to PIP_2-containing membranes for rapid and efficient exocytosis.

Results

The RIM C_2B domain is crucial for synaptic vesicle release

Based on the high conservation of the RIM C_2B domain (Wang and Südhof, 2003), the strong behavioral defects upon RIM C_2B deletion in *C. elegans* (Koushika et al., 2001), and the general importance of C_2 domains in vesicle fusion (Südhof, 2013), we hypothesized that RIM C_2B is critical for synaptic vesicle release. To test this hypothesis, we expressed full length RIM1α (RIM WT) and a RIM1 mutant lacking the C_2B domain (RIM ΔC_2B) in cultured hippocampal neurons obtained from RIM1/2 conditional knockout mice (Figure 1B). In this preparation, the *Rims1* and *Rims2* genes contain essential exons flanked by *loxp* sites, and we expressed Cre recombinase from a lentivirus to remove all RIM1 and RIM2 isoforms (cDKO) (Kaeser et al., 2008, 2011). Control neurons are neurons from the same litter infected with a lentivirus that expressed an inactivated variant of Cre recombinase (Kaeser et al., 2008). We delivered RIM using separate lentiviruses because bicistronic

Author Manuscript Author Manuscript Author Manuscript Author Manuscript

expression of Cre and rescue proteins, as described before (Kaeser et al., 2011), is impractical for full length RIM1α due to the packaging size limit of lentiviruses. This approach yielded reliable removal of endogenous RIM, and exogenous RIM expression reached levels above wild type control neurons (Figure S1B). RIM WT expression fully rescued the amplitude of action potential evoked γ-aminobutyric acid (GABA)-ergic inhibitory postsynaptic currents (IPSCs) and nearly completely restored paired pulse ratios (PPRs, Figures 1C–1F), which are inversely correlated with vesicular release probability (*p*) (Zucker and Regehr, 2002). RIM ΔC_2B was expressed at levels comparable to RIM WT (Figure S1B), but showed no significant increase in the IPSC amplitude compared to cDKO neurons (Figures 1C and 1D). Furthermore, the PPR of RIM ΔC_2B was indistinguishable from cDKO at all intervals tested (Figures 1E and 1F). Thus, the RIM C_2B domain is necessary to enhance *p,* and removing C_2B abolishes rescue activity. Importantly, expression of RIM WT or RIM ΔC_2B in control neurons did not enhance or suppress release (Figures S1C–S1H), indicating that the effects in the rescue conditions are not due to overexpression or dominant negative roles. Furthermore, using the same experimental design, we found that deletion of RIM C_2A has no strong effect on synaptic transmission (Figures S1I–S1P). We conclude that the C_2B domain of RIM1 is crucial to set *p* at inhibitory synapses.

RIM C_2B is not necessary for localizing RIM to the active zone

We hypothesized that the severe phenotype of RIM ΔC_2B rescue might be due to perturbed recruitment of RIM ΔC_2B to the active zone. To test this hypothesis, we performed stimulated emission depletion (STED) microscopy on cultured neurons stained for the inhibitory synapse marker vGAT, the active zone marker Bassoon, and RIM (Figures 1G–1M and S2A). RIM signals in control synapses co-localized well with Bassoon. To measure RIM levels at active zones, we detected Bassoon objects within vGAT positive synapses, and measured RIM staining intensities within Bassoon objects. While RIM rescue levels appeared slightly higher than control, we observed no difference between RIM WT and RIM ΔC_2B (Figure 1H). In addition, no differences were found in the average Bassoon intensity, or the size of Bassoon objects (Figures 1I, 1J). To evaluate whether RIM ΔC_2B localized normally within the presynaptic terminal, we selected synapses in side view, defined as a cluster of vGAT positive vesicles that contains an elongated band of Bassoon at the edge of the cluster (Wong et al., 2018). We then measured the staining intensity profile along a 250 nm wide rectangle perpendicular to the Bassoon band (Figure 1K), and aligned all profiles to the peak Bassoon intensity. Peak intensity of RIM co-localized well with Bassoon in control neurons, and peak intensity of RIM WT and RIM ΔC_2B rescue proteins, while higher in intensity than endogenous RIM, did not shift relative to Bassoon (Figure 1L). The Bassoon signal did not change across conditions (Figure 1M). Despite complete absence of RIM in Western blotting (Figure S1B, and (Kaeser et al., 2011)), a small peak remained in cDKO in STED, similar to the 25% background with the same antibody in confocal analyses (Wang et al., 2016). These data establish that the RIM C_2B domain is not required for RIM active zone localization.

The RIM C_2B domain mediates a new function of RIM

We next assessed whether the RIM C_2B domain participates in the two established RIM functions, which are synaptic vesicle priming via recruitment of Munc13 (Andrews-Zwilling

Author Manuscript Author Manuscript Author Manuscript Author Manuscript

et al., 2006; Camacho et al., 2017; Deng et al., 2011), and enhancing Ca^{2+} influx by tethering of presynaptic Ca^{2+} channels (Han et al., 2011; Kaeser et al., 2011; Muller et al., 2012). To test if RIM C_2B is required to recruit Munc13 to the active zone, we quantified Munc13 levels within Bassoon objects using STED microscopy (Figures 2A–2D and S2B–S2D). RIM cDKO led to a reduction in Munc13 at the active zone, consistent with the reduction of Munc13 in RIM cDKO neurons (Deng et al., 2011). Strikingly, RIM ΔC_2B and RIM WT rescue led to Munc13 levels slightly above control (Figure 2B), and the Munc13 peak intensity localized to the active zone in control as well as rescue conditions (Figure 2C). We next measured the size of the primed vesicle pool (readily releasable pool, RRP) by the application of hypertonic sucrose (Rosenmund and Stevens, 1996) and observed that RIM WT and RIM ΔC_2B rescued RRP size to similar levels (Figures 2E and 2F). Thus, despite the failure to rescue action potential induced release, RIM ΔC_2B is able to recruit Munc13 to active zones and to restore the RRP.

To test whether the RIM C_2B domain contributes to presynaptic Ca^{2+} influx, we loaded individual cells with the low affinity Ca^{2+} indicator Fluo-5F through a patch pipette and measured Ca^{2+} influx in individual presynaptic boutons in response to a single action potential induced by a brief somatic current injection (Figures 2G and 2H). Both RIM WT and RIM ΔC_2B significantly increased presynaptic Ca^{2+} influx compared to cDKO, and no difference was observed between the two rescue conditions. Thus, the C_2B domain is not required to boost presynaptic Ca^{2+} influx. Taken together, these data establish that the RIM C_2B domain is critical to enhance p, but it does so independent of the known roles of RIM in vesicle priming or Ca^{2+} influx.

RIM C_2 domains bind to PIP_2

What is the function of RIM C_2B domains in synaptic transmission? The RIM C_2B domain contains a lysine-rich polybasic sequence that is highly conserved among C_2 domains, and this sequence mediates binding to the phospholipid PIP_2 in several other C_2 domains (reviewed in (Corbalan-Garcia and Gómez-Fernández, 2014)). To test if RIM1 C_2B binds to PIP_2, we performed liposome binding assays in which we measured co-sedimentation of purified C_2B with heavy liposomes (Figures 3A and 3B). While we detected only weak binding of C_2B to liposomes composed of phosphatidylcholine (PC) and phosphatidylserine (PS), addition of PIP_2 enhanced co-sedimentation of the C_2B domain with liposomes, suggesting direct binding of C_2B to PIP_2. Changing the surface charge of the liposomes by adding extra PS did not alter the amount of binding, suggesting that the interaction is specific for PIP_2 and not simply mediated by changes in membrane charge (Figures 3A and 3B). We then tested how different lipid composition of the liposomes influenced binding of the RIM C_2B domain using co-floatation assays. We found that the binding was almost entirely specific for PIP_2 (Figure 3C), and other lipids, including the phosphoinositides PI and PIP, only showed weak binding.

We next used nuclear magnetic resonance (NMR) spectroscopy and a water soluble PIP_2 analogue (diC4-PIP_2) to characterize its interaction with the RIM1 C_2B domain. ^{1}H-^{15}N heteronuclear single quantum coherence (HSQC) spectra of C_2B in the absence and presence of 100 μM diC4-PIP_2 revealed specific cross-peak shifts (Figure 3D),

Author Manuscript Author Manuscript Author Manuscript Author Manuscript

demonstrating a direct interaction. To measure the binding affinity, we repeated the experiment at increasing concentrations of diC4-PIP_2 (0–250 μM), which resulted in progressive shifts of the same cross-peaks (Figure 3E). We fitted the perturbations of individual chemical shifts from the cross-peaks that were most affected by diC4-PIP_2 binding as a function of diC4-PIP_2 concentration, and obtained K_ds that ranged from 32 to 79 μM (Figure 3F). The K_d values are within the range of those found for other C_2 domains (Van den Bogaart et al., 2012; Montaville et al., 2008), and the variability is expected considering that some shifts are relatively small. These results establish RIM1 C_2B as a PIP_2 binding module.

It was previously suggested that C_2B forms a weak dimer via an interface that partly overlaps with the polybasic sequence (Guan et al., 2007), which thus might interfere with PIP_2 binding. Using analytical ultracentrifugation, we found that the C_2B homodimer affinity was very weak (K_d ~ 3 mM, Figure 3G), which makes it very unlikely to be physiologically relevant. Additionally, we found that the addition of PIP_2 did not change the line widths of methyl resonances of 1D ^{1}H-NMR spectra of RIM1 C_2B, indicating that PIP_2 does not change the very weak dimerization of C_2B (Figure 3H).

We finally characterized the PIP_2 binding of RIM1 by analyzing its C_2A domain with the same assays (Figures S3A–S3F). We observed a specific interaction of C_2A with PIP_2-containing liposomes, and titrations monitored by ^{1}H-^{15}N HSQC spectra yielded a K_d value that was comparable to those measured for C_2B. Thus, RIM1 can bind to PIP_2-containing membranes via its C_2A and C_2B domains.

Distinct PIP_2 binding modes of the RIM C_2 domains

We next designed mutations to interfere with PIP_2 binding. Since RIM1 C_2B contains a polybasic sequence that is conserved among PIP_2-binding C_2 domains (Figure S3G), we based our mutations on homologous PIP_2-binding sequences (Corbalan-Garcia and Gómez-Fernández, 2014). Using lipid co-sedimentation, we found that mutating single or multiple lysine (K) residues to glutamates (E) in the conserved polybasic sequence strongly impaired PIP_2 binding (Figures 4A and 4B). From these mutants, we selected a double mutant in which K1513 and 1515 were mutated to E (K1513/1515E, named C_2B 2E from hereon) for further analysis, because these lysines are conserved and have been well characterized in homologous C_2 domains in biochemical and functional assays (Figures 4C and 4D) (Van den Bogaart et al., 2012; Groffen et al., 2010; Guerrero-Valero et al., 2009; Li et al., 2006). The ^{1}H-^{15}N HSQC spectrum of C_2B 2E exhibited only small perturbations compared to that of WT C_2B (Figure 4E), showing that the mutation did not perturb the folding of the domain. Importantly, no cross peak shifts were observed after the addition of diC4-PIP_2 in RIM1 C_2B 2E (Figure 4F), demonstrating that the 2E mutation abolished PIP_2 binding.

The polybasic sequence is only partially conserved in RIM1 C_2A (Figure S3G). When we tested whether the lysine and arginine (K809 and R811) residues in C_2A, at corresponding positions to K1513 and K1515 in C_2B, were necessary for PIP_2 binding of C_2A, we found that mutating them to glutamates (KR mutant) did not completely abolish diC4-PIP_2 binding (Figures S4A and S4B). Instead, RIM1 and RIM2 C_2A contain two unique arginines at the bottom of the β-sandwich (R834 and R835, Figures S3G and S4A) that could potentially

Author Manuscript Author Manuscript Author Manuscript Author Manuscript

bind to PIP_2, and mutation of one of these arginines has been associated with autosomal cone-rod dystrophy in human genetic studies (Johnson et al., 2003). ^{1}H-^{15}N HSQC spectra showed that mutation of both arginines to glutamate (C_2A 2E mutant) abolished binding of RIM1 C_2A to diC4-PIP_2 without perturbing its folding (Figures S4C and S4D). Hence, RIM1 C_2 domains, and likely other C_2 domains, can bind to PIP_2 through different motifs located at distinct regions of the β-sandwich.

Finally, we tested if the binding of the RIM C_2 domains to phosphoinositides is restricted to PIP_2 phosphorylated at the 4 and 5 positions at the inositol ring ($PI(4,5)P_2$). We found that isomers other than $PI(4,5)P_2$, as well as PIP_3, induced only weak or no binding of C_2B to liposomes in lipid co-sedimentation assays (Figures S4E – S4H). Hence, phosphoinositide binding of RIM C_2B is mostly specific for $PI(4,5)P_2$. Importantly, the 2E mutation of either C_2A or C_2B inhibited binding to all PIP_2 isomers.

The polybasic region of RIM C_2B is critical for synaptic vesicle release

To investigate the functional importance of the interactions of RIM C_2 domains with PIP_2, we generated a RIM1 mutant that harbors the 2E mutations of both C_2A and C_2B (RIM 4E, Figure 5A). RIM 4E was expressed at levels comparable to RIM WT, was efficiently recruited to synapses, and restored the priming deficit of RIM cDKO (Figures S5A–S5F). The amplitude of evoked IPSCs, however, was severely reduced compared to control and RIM WT rescued cells, and was statistically indistinguishable from that of cDKO neurons (Figures 5A–5C). In addition, RIM 4E showed no rescue of PPRs (Figures 5D and S5G) or release induced by brief action potential trains (10 action potentials at 10Hz, Figures S5H and S5I). Thus, the RIM 4E mutant did not rescue *p* and phenocopied the RIM ΔC_2B rescue experiments (Figures 1, 2).

To test if the phenotype of RIM 4E is due to mutations in C_2A, C_2B, or both, we generated variants of RIM in which only C_2A (RIM A2E) or C_2B (RIM B2E) was mutated (Figure 5E). As observed with RIM 4E, RIM A2E or B2E mutants expressed normally (Figure S5J). While RIM A2E led to significant rescue of the IPSC amplitude, RIM B2E did not show any rescue (Figures 5F and 5G). Similarly, RIM A2E rescued PPRs as efficiently as RIM WT, but RIM B2E did not display any rescue at all (Figure 5H and Figure S5K). Thus, we could not detect a statistically significant defect in synaptic transmission upon abolishing PIP_2 binding to C_2A, consistent with the finding that removing the C_2A domain does not impair rescue (Figures S1H–S1P). However, mutating the polybasic region in RIM C_2B alone leads to absence of rescue. This establishes a central role for this motif in synaptic vesicle fusion.

Known protein interactions of RIM C_2B do not mediate its role in exocytosis

Is the effect of the C_2B 2E mutation solely due to a loss of PIP_2 binding, or does the mutation affect other molecular interactions as well? Previous studies have proposed that multiple proteins interact with RIM1 C_2B, including Liprin-α (Schoch et al., 2002), synaptotagmin-1 (Coppola et al., 2001; Schoch et al., 2002), the SNARE proteins syntaxin-1 and SNAP-25 (Coppola et al., 2001) and β subunits of Ca^{2+} channels ($Ca_V\beta$, Kiyonaka et al., 2007), although several of these interactions could not be reproduced by NMR spectroscopy (Guan et al., 2007). To test if C_2B 2E mutations interfere with these interactions, we

Author Manuscript Author Manuscript Author Manuscript Author Manuscript

performed GST affinity purifications from mouse brain, and detected potential interactors by western blotting. We could not detect any binding to SNAREs and $Ca_V\beta4$ (Figure 6A). To further characterize potential binding to SNAREs, we acquired ^{1}H-^{15}N HSQC NMR spectra of ^{15}N-labeled C_2B WT without or with unlabeled syntaxin-1 or SNAP-25 (Figures S6A and S6B). No binding between C_2B and these SNARE proteins was observed. We did observe weak Ca^{2+}-dependent binding of C_2B to synaptotagmin-1 in GST affinity purification, which was not affected in C_2B 2E (Figure S6C) and hence is unlikely to explain the strong impairment in exocytosis of RIM1 C_2B 2E. Furthermore, we suspect that this binding is largely artifactual due to polyacidic impurities upon purification of GST-RIM1 C_2B (Figures S6D–S6E), which was previously observed for synaptotagmin C_2 domains (Ubach et al., 2001). In line with this conclusion, this interaction could not be observed using purified protein preparations and NMR spectroscopy (Guan et al., 2007).

As reported previously (Schoch et al., 2002), RIM1 C_2B bound to Liprin-α in GST affinity purifications, and we found that the 2E mutation in C_2B did not impair binding (Figure 6A). While testing binding of the C_2B domains of RIM3 and RIM4, two short RIM homologues that have no known function in synaptic transmission, we found that neither bound to Liprin-α (Figure 6A). To further characterize the RIM C_2B - Liprin-α interaction, we performed affinity binding assays using the Liprin-α3 LH1 or LH2 domain fused to GST (GST-Liprin-α3-LH1 and -LH2) on beads, and His-tagged C_2B variants in solution, which do not show the ribonucleic acid contaminants that lead to artifacts using GST-C_2 domains (Figures S6D and S6E). We found that RIM1 C_2B, RIM1 C_2B 2E and RIM2 C_2B bound specifically to LH2 (Figures 6B and 6C). In contrast, neither RIM3 C_2B nor RIM4 C_2B showed any appreciable binding. Thus, the interaction of RIM1 C_2B with Liprin-α is not affected by the 2E mutation, and RIM3 and RIM4 C_2B do not bind to Liprin-α. In contrast, the polybasic sequence is fully conserved between RIM1, -3 and -4 C_2B (Figure S3G), and we found that RIM1, -3 and -4 C_2B bind to PIP_2 to a similar extent in lipid co-sedimentation experiments (Figures 6D and 6E). Thus, RIM3 and RIM4 C_2B bind to PIP_2 but not to Liprin-α.

One possible scenario for the function of RIM C_2B is that it recruits Liprin-α to PIP_2-enriched membranes, and that synergistic binding to Liprin-α and PIP_2 is required to control synaptic transmission. Another scenario is that the C_2B domain does not work autonomously in synaptic transmission, but tethers the biochemical activities of other RIM domains to PIP_2 containing membranes. A previous study supports the latter possibility, because expression of the RIM2 C_2B domain alone did not confer rescue of synaptic transmission (Kaeser et al., 2012). To directly test whether Liprin-α binding is involved in rescue, we made use of the finding that RIM3 and RIM4 C_2B do not bind to Liprin-α, but bind to PIP_2. We created hybrid constructs of RIM1 where the C_2B domain is replaced with that of RIM3 (RIM 1–3) or RIM4 (RIM 1–4), and tested their effect on synaptic transmission (Figures 6F–6I). RIM 1–3 and RIM 1–4 were expressed at levels comparable to RIM WT (Figures S7A). RIM 1–4 fully rescued evoked release as well as PPRs, indistinguishable from RIM WT rescue (Figures 6G–6I and S7B). These findings directly demonstrate that Liprin-α binding to C_2B is not required for rescue. Somewhat surprisingly, RIM 1–3, while having biochemical properties identical to RIM 1–4 in terms of PIP_2 and Liprin-α binding, showed only partial rescue of evoked release, and strongly diminished rescue of PPRs (Figures 6G–6I). These observations suggest that C_2B may have additional unidentified roles that are not conserved

Author Manuscript Author Manuscript Author Manuscript Author Manuscript

in RIM3 C_2B. To further test whether C_2B might have a second activity besides PIP_2 binding, we exchanged C_2B with another PIP_2-binding C_2 domain. The C_2C domain of extended synaptotagmin-2 has a polybasic sequence nearly identical to RIM C_2B (Figures 4C and S3G), and binds to PIP_2 but not Ca^{2+} (Giordano et al., 2013). The resulting hybrid construct (RIM ΔC_2B–C_2C, Figure S7C) was efficiently expressed in cultured neurons and rescued vesicle priming (Figures S7D–S7F), but failed to rescue evoked release as well as PPRs (Figures S7G–S7J). We conclude that RIM1 C_2B has likely an additional function in synaptic transmission, or, more trivially, that artificially fusing RIM3 C_2B or extended synaptotagmin-2 C_2C with RIM1 affects the packing of the C-terminal C_2 domain against the rest of the protein, which in turn reduces rescue activity.

C_2B needs to be attached to RIM to mediate rescue

Our results thus far suggest that C_2B tethers RIMs known roles in release to membranes that contain PIP_2. However, it is also possible that C_2B has an autonomous function at the active zone, and does not need to be attached to the N-terminal RIM domains to increase synaptic vesicle fusion. To distinguish between these possibilities, we expressed RIM C_2B alone or together with RIM ΔC_2B (RIM ΔC_2B + C_2B, Figures 7A and S7K), and measured the effect on synaptic transmission. Strikingly, we observed no rescue of IPSC amplitudes or PPRs by RIM C_2B alone or by RIM ΔC_2B + C_2B, but only RIM WT was sufficient for rescue (Figures 7B–7D and S7L). These results indicate that C_2B needs to be attached to the N-terminal domains of RIM to execute its role in synaptic vesicle release, directly establishing a tethering function.

RIM C_2B has a universal role in synaptic transmission

The results discussed so far demonstrate that RIM1 C_2B has a crucial function in regulating *p* at inhibitory synapses. Is this function unique to GABAergic synaptic transmission, or shared among many synapses? To address this, we recorded *N*-methyl-D-aspartate (NMDA) receptor mediated excitatory postsynaptic currents (EPSCs) in cultured hippocampal neurons in control neurons, cDKO neurons, and cDKO neurons rescued with full length RIM or RIM ΔC_2B. When measuring single evoked EPSC amplitudes, we found that RIM ΔC_2B did not show any rescue (Figures 7E and 7F). Additionally, RIM ΔC_2B failed to rescue PPRs (Figures 7G and S7M), indicating a defect in *p* at excitatory synapses. These results establish that the role of C_2B is not restricted to inhibitory synapses, but instead may be important at diverse synapses throughout the brain.

Discussion

The presynaptic active zone controls vesicle docking, priming and the anchoring of Ca^{2+} channels. The fusion reaction itself is mediated by SNARE proteins (Jahn and Fasshauer, 2012; Südhof, 2013) and requires PIP_2 in the target membrane (Di Paolo et al., 2004). We found here that both C_2 domains of RIM bind to PIP_2 and that the interaction between the C_2B domain and PIP_2 is essential for RIM's role in synaptic vesicle fusion. Importantly, the C_2B domain cannot act autonomously to mediate this role, but needs to be attached to the other RIM domains. In contrast to interactions of other presynaptic C_2 domain proteins with PIP_2, PIP_2 interactions of RIM are not controlled by Ca^{2+}-binding to RIM C_2B, and may

Author Manuscript Author Manuscript Author Manuscript Author Manuscript

thus fulfill constitutive, activity-independent functions. We propose that the C_2B domains cluster the vesicle priming and Ca^{2+} channel tethering functions of RIM to PIP_2 in the target membrane to enable fast and efficient exocytosis (Figure 7H).

PIP_2 binding of RIM C_2 domains

We found that RIM1 C_2B binds specifically to PIP_2-containing membranes via a binding region that is similar to those of homologous C_2 domains (Figures 3 and 4, and (Corbalan-Garcia and Gómez-Fernández, 2014)). Indeed, as observed previously for other PIP_2 binding C_2 domains (Van den Bogaart et al., 2012; Guerrero-Valero et al., 2009; Li et al., 2006), mutations in the polybasic sequence of RIM1 C_2B (K1513E, K1515E) abolish binding to PIP_2. We further found that RIM C_2A binds to PIP_2. Surprisingly, this interaction was largely mediated by R834 and R835 located at the bottom of the β-sandwich, an area that has not been implicated in PIP_2 binding of other C_2 domains. This finding suggests a new mode of PIP_2 binding, which may also be employed by other C_2 domains. While we identified essential roles for PIP_2 binding to C_2B in synaptic transmission, we could not detect a strong effect of PIP_2 binding to the C_2A domain in synaptic transmission at hippocampal synapses. It is interesting, however, that a point mutation in R834 is associated with a form of cone-rod dystrophy (CORD7), a form of late onset blindness (Johnson et al., 2003). Thus, the C_2A-PIP_2 interaction may play important roles that are either too mild to detect in our experimental paradigm, act on processes not tested here, or may be more pronounced in other synapses.

RIM C_2B is critical for action potential mediated release

RIM ΔC_2B did not rescue action potential evoked vesicle release in RIM cDKO, demonstrating that C_2B is essential for the function of RIM in synaptic transmission (Figures 1 and 2). This is in line with a study in *C. elegans*, where ΔC_2B phenocopies behavioral impairments caused by deletion of RIM (Koushika et al., 2001). The strong defect in PPR, contrasted by rescue of vesicle priming and Munc13 levels and localization (Figure 2), establishes a defect in vesicular release probability *p*. RIM boosts Ca^{2+} influx (Han et al., 2011; Kaeser et al., 2011; Muller et al., 2012), which may explain a reduction in *p*. Previously, RIM C_2B was shown to inhibit voltage dependent Ca^{2+} channel inactivation to enhance Ca^{2+} currents in transfected, non-neuronal cells (Kaeser et al., 2012; Kiyonaka et al., 2007; Uriu et al., 2010), suggesting a direct role for C_2B in presynaptic Ca^{2+} influx. However, our experiments establish that RIM C_2B domains do not boost *p* through enhancing Ca^2 -influx. First, we found that RIM ΔC_2B rescues Ca^{2+} influx (Figure 2). Second, train stimulation, which leads to high residual Ca^{2+} in nerve terminals, fails to boost vesicle fusion in RIM 4E expressing neurons, indicating that the role of C_2B is downstream of Ca^{2+} influx (Figure S5). Third, RIM C_2B domains alone do not increase action potential triggered release or its Ca^{2+} dependence in RIM cDKO neurons (Figure 7 and (Kaeser et al., 2011, 2012)). Finally, the effect in heterologous cells was observed for all RIMs, including RIM3 (Uriu et al., 2010), but we found that substitution of RIM1 C_2B with RIM3 C_2B did not fully rescue *p* (Figure 6). Thus, RIM C_2B does not boost Ca^{2+} entry to enhance *p*. Importantly, RIM cDKO at the Calyx of Held leads to reduced Ca^{2+} sensitivity of fusion when Ca^{2+} entry is bypassed with Ca^{2+} uncaging (Han et al., 2011), supporting that roles for

Author Manuscript Author Manuscript Author Manuscript Author Manuscript

RIM in *p* independent of Ca^{2+} entry exist. We conclude that C_2B mediates a new function of RIM, independent of its activities in vesicle docking, priming and Ca^{2+} entry.

Roles for RIM C_2B binding to PIP_2 in action potential triggered release

In rescue experiments using mutations in the polybasic sequence of C_2B, we identified a critical role for PIP_2 binding to the RIM C_2B domain for action potential induced release (Figure 5). Could other interactions of the RIM C_2B domain contribute to the function of C_2B in vesicle fusion? As outlined above, it is unlikely that the previously identified interaction with β subunits of Ca^{2+} channels contributes via boosting Ca^{2+} influx. The RIM1 C_2B domain was also identified to bind to Liprin-α proteins (Schoch et al., 2002), and this interaction was not affected by the C_2B 2E mutation (Figure 6). Remarkably, Liprin-α did not bind to RIM4 C_2B, but replacing RIM1 C_2B with the C_2B domain of RIM4 fully rescued fusion. Hence, binding of Liprin-α to RIM is either not important for neurotransmitter release, or functional redundancy with other RIM interactions masks important roles for Liprin-α RIM C_2B domain interactions.

Surprisingly, substitution with the RIM3 C_2B domain, which, like RIM4 C_2B, binds PIP_2 but not Liprin-α, led to incomplete rescue of synaptic transmission (Figure 6). In addition, exchanging C_2B with the C_2C domain of extended synaptotagmin-2, which, like C_2B, binds PIP_2 but not Ca^{2+} (Giordano et al., 2013), failed to rescue *p* or IPSC amplitudes (Figure S7). Thus, substituting C_2B with another PIP_2-binding C_2 domain is insufficient, indicating that RIM1 C_2B has additional roles in vesicle fusion that are also present in RIM4 C_2B. Interestingly, our data show that C_2B alone is insufficient to boost fusion in cDKO neurons (Figure 7 and (Kaeser et al., 2011, 2012)), and that C_2B must be connected to the N-terminal RIM domains to rescue exocytosis (Figure 7). This indicates that its role at the active zone requires close proximity to the other RIM domains and their binding partners, and it is possible that C_2B engages in intramolecular interactions with other RIM domains.

Does RIM C_2B localize synaptic vesicle priming and Ca^{2+} influx to PIP_2-containing membranes?

PIP_2 is required at the target membrane for efficient vesicle fusion (Hay et al., 1995; Milosevic et al., 2005; Di Paolo et al., 2004). While the exact distribution of PIP_2 at the active zone is unknown, studies in non-neuronal cells showed that PIP_2 is clustered in small domains within the plasma membrane (van den Bogaart et al., 2011; Honigmann et al., 2013; Laux et al., 2000). Functions of many core components of the synaptic vesicle fusion machinery depend on interactions with PIP_2, for example those of synaptotagmin, syntaxin, Munc13 and Ca^{2+} channels (Bai et al., 2004; van den Bogaart et al., 2011; Li et al., 2006; Shin et al., 2010; Suh et al., 2010). Multiple additional proteins that regulate synaptic exocytosis bind to PIP_2, including CAPS, Doc2, PKC, and Rabphilin, and endocytosis is also dependent on PIP_2 (Koch and Holt, 2012; Lauwers et al., 2016). Hence, optimal fusion requires co-localization of PIP_2 with these proteins, and mis-targeting of release machinery away from PIP_2-containing membranes would lead to impaired release with multiple proteins operating at sub-optimal capacity.

Author Manuscript Author Manuscript Author Manuscript Author Manuscript

We propose that RIM C_2B domains target release machinery to PIP_2-containing membranes (Figure 7H). This targeting mechanism could have several important implications for synaptic vesicle exocytosis. If PIP_2 is present at the active zone in small clusters, as has been observed in non-neuronal cells (Aoyagi et al., 2005; van den Bogaart et al., 2011; Honigmann et al., 2013), this could provide for nanoscale scaffolding at PIP_2-rich fusion sites to integrate the functions of RIM, and potentially its PIP_2-dependent interaction partners, for efficient docking, priming and Ca^{2+} triggering. Recent findings provide further support for this model. Within an active zone, synaptic vesicle exocytosis is restricted to a few sites (Maschi and Klyachko, 2017; Tang et al., 2016). These sites align in a nano-columnar structure with postsynaptic receptor clusters and contain RIM as a central component. Remarkably, the diameter of these RIM clusters is ~80 nm (Tang et al., 2016), very similar to the diameter of syntaxin-associated PIP_2 clusters, which was determined to be 73 nm in non-neuronal secretory cells (van den Bogaart et al., 2011). The exact distribution of PIP_2 within an active zone and the underlying clustering mechanisms are currently unknown because the available tools have not allowed measuring PIP_2 clustering at synapses. In the model in which RIM targets release to PIP_2-containing fusion sites, we favor that PIP_2 clusters RIM and its activities in exocytosis because there are likely many more PIP_2 molecules than RIM molecules in a nerve terminal. But it is possible that RIM has an active role in generating PIP_2 clusters, or that PIP_2 activates other RIM activities. Ultimately, the functional effects of these alternative possibilities are similar: they all lead to fusion sites where essential activities of RIM and PIP_2 are tethered to one another for efficient exocytosis.

Because the extent of nanoscale clustering of PIP_2 at the active zone is not well known, other potential roles of PIP_2-RIM interactions need to be considered. It is well established that PIP_2 defines the plasma membrane identity (Di Paolo and De Camilli, 2006) independent of how it is clustered. Hence, it is possible that the targeting function of RIM-PIP_2 interactions is necessary to assemble fusion machinery in the correct orientation for efficient release, or that this interaction provides a proofreading mechanism to ensure that exocytosis occurs at the correct target membrane. The apparent specificity of C_2B for the $PI(4,5)P_2$ isomer (Figure S4) would be in line with the latter model, as this isomer is almost exclusively present at the plasma membrane (Di Paolo and De Camilli, 2006). Finally, because RIM C_2B has additional roles in fusion (Figures 6 and S7), it is possible that these roles are activated by PIP_2. In a similar fashion, Ca^{2+}-binding to synaptotagmin-1 C_2B is likely activated by PIP_2 (Bai et al., 2004; Van den Bogaart et al., 2012).

We have identified an unexpected, important role for RIM C_2B in the control of synaptic vesicle exocytosis. Our data suggest that the function of RIM at the active zone reaches beyond docking, priming and tethering of Ca^{2+} channels, but directly regulates the efficiency of fusion by interacting with essential membrane lipids. RIM and PIP_2 have important roles in fusion outside the nervous system (Hay et al., 1995; Milosevic et al., 2005; Yasuda et al., 2010), and many additional C_2 domain proteins are Ca^{2+} independent, but have polybasic sequences in their C_2 domains similar to RIM. Hence, the constitutive tethering of C_2 domain scaffolds to PIP_2-rich membranes may provide for a mechanism across diverse secretory pathways to target exocytosis to specific membrane domains.

Author Manuscript Author Manuscript Author Manuscript Author Manuscript

STAR Methods

Contact for reagent and resource sharing

Requests for reagents and resource sharing should be directed to the Lead Contact, Pascal S. Kaeser, at kaeser@hms.harvard.edu

Experimental models and subject details

Mice—RIM1/2 conditional knockout mice were previously described (Kaeser et al., 2011) and were maintained as homozygote lines in which the *Rims1* gene (RRID:IMSR_JAX:015832 (Kaeser et al., 2008)) and the *Rims2* gene (RRID:IMSR_JAX:015833 (Kaeser et al., 2011)) contained essential exons flanked by *loxp* sites. All animal experiments were approved by the Harvard University Animal Care and Use Committee.

Neuronal cell cultures and lentiviral infection—Dissociated high-density hippocampal cultures were prepared from newborn RIM1/2 conditional double knockout mice of either sex as described (Kaeser et al., 2008; Maximov et al., 2007). Lentiviruses were produced in HEK293T cells. HEK cells were maintained in DMEM supplemented with 10% fetal bovine serum and 1% penicillin/streptomycin and were split every 2 days to maintain optimal growth rate. For virus production, HEK cells in neuronal culture media were transfected using Fugene (Promega) with 3rd generation lentiviral packaging plasmids (REV, RRE and VSV-G) and a separate lentiviral plasmid (FSW or FUGW) encoding the recombinant gene of interest. After 48 h, the culture medium was harvested and centrifuged for 5 min at 700 × *g*, and the supernatant was used immediately for infection. Neuronal cultures were infected at 4 days in vitro (DIV) with lentiviruses expressing GFP-Cre with enhanced nuclear localization driven by a ubiquitin (for electrophysiology) or synapsin promoter (for Ca^{2+}-imaging) to generate cDKO neurons or an inactivate, truncated variant of GFP-Cre to generate control neurons (Kaeser et al., 2011). For rescue expression of full length RIM or mutant RIM, cultures were infected with a separate rescue virus containing ubiquitin-promotor driven RIM open reading frame with an HA tag immediately following the PxxP motif (plasmid pAJ14063, (Kaeser et al., 2011)).

Method details

Lentiviral rescue constructs—To obtain a RIM ΔC_2B construct, full length RIM1α was truncated at the residue immediately preceding C_2B, following the definition of (Guan et al., 2007), the last residues being …FLDGL-stop (pAJ15020). In all constructs where C_2B is substituted with another domain, the substituting domain was fused directly to RIM ΔC_2B without additional linker sequences. RIM3 C_2B (residues GPAQI…SPSCS, pAJ15019) and RIM4-C_2B (residues GPAQF…CGERS, pAJ15032) were obtained from rat, Extended Synaptotagmin-2 C_2C (residues RLRQL…PQAMT, Addgene #66831, (Giordano et al., 2013), pAJ17016) from human. For co-expression of RIM ΔC_2B and C_2B in Figure 8, RIM1 C_2B (residues GPAQL…PCIRS-stop) was fused to Cre with a 2A sequence (pAJ17015). Successful expression of both open reading frames was confirmed by western blotting. To obtain RIM1 ΔC_2A, the sequence between residues DAPQV…HDESS in RIM1α was substituted with a short linker sequence (GSGA, pAJ17013)). Point mutations in C_2A and C_2B were generated by site-directed mutagenesis (pAJ14064, pAJ14065,

Author Manuscript Author Manuscript Author Manuscript Author Manuscript

pAJ14066). Expression of rescue constructs was confirmed by western blotting for every culture.

Electrophysiology—Whole-cell patch-clamp recordings were performed in cultured hippocampal neurons at DIV14-17 as described in (Maximov et al., 2007; Wang et al., 2016) at room temperature. Extracellular solution contained (in mM) 140 NaCl, 5 KCl, 2 $CaCl_2$, 2 $MgCl_2$, 10 HEPES (pH 7.4) and 10 Glucose. Borosilicate glass pipettes (2.5 – 4.5 MΩ) were filled with intracellular solution containing (in mM) 40 CsCl, 90 K-gluconate, 1.8 NaCl, 1.7 $MgCl_2$, 3.5 KCl, 0.05 EGTA, 10 HEPES (pH 7.4), 2 ATP-Mg, 0.4 GTP-Na_2, 10 phosphocreatine, 4 QX314-Cl. Cells were clamped at −70 mV, with R_{series} < 15 MΩ, and R_{series} was compensated online until R_{access} = 0.6 – 1.1 MΩ (typically 50–70%). Action potential-evoked IPSCs were elicited by local electric stimulation and recorded in extracellular solution supplemented with 20 μM 6-cyano-7-nitroquinoxaline-2,3-dione (CNQX) and 50 μM (2R)-amino-5-phosphonovaleric acid (D-AP5). Evoked EPSCs were recorded in extracellular solution supplemented with 20 μM CNQX and 20 μM picrotoxin (PTX), and cells were clamped at +40 mV. For RRP measurements, 500 mM hypertonic sucrose was applied for 10 seconds by local perfusion (Rosenmund and Stevens, 1996), in the presence of 20 μM CNQX, 50 μM D-AP5 and 1 μM tedrodotoxin (TTX). The integral of the first 10 s of the response was used as measure of the RRP. Data were acquired using a Multiclamp 700B amplifier and a Digidata 1550 digitizer, recorded at 10 kHz, and filtered at 2 kHz. Data were analyzed using pClamp and custom written programs in MATLAB. For all electrophysiological experiments and analyses, the experimenter was blind to the experimental condition.

Ca^{2+} imaging—Imaging of presynaptic Ca^{2+}-transients was performed as described in (Wang et al., 2016) with minor modifications. Neurons were recorded at DIV14-16 with whole-cell patch clamp electrophysiology at room temperature in extracellular solution supplemented with 20 μM CNQX, 50 μM D-AP5 and 20 μM PTX. Intracellular solution contained (in mM) 140 K-Gluconate, 0.1 EGTA, 2 $MgCl_2$, 4 Na_2ATP, 1 NaGTP, 0.3 Fluo5-F, 0.03 AlexaFluor-647 10 HEPES (pH 7.4). Because of the limited time window during which this experiment needs to be done and its laborious nature, we could only analyze three conditions at a time, and hence we compared RIM cDKO neurons to cDKO neurons rescued with RIM WT or RIM ΔC_2B. After filling for 7 minutes in current clamp (V_m < −50 mV at I = 0 pA), boutons were identified in the Alexa channel, based on their typical bead-like morphology. After 10 minutes of filling, cells were held at V_m = −60 mV, and action potentials were triggered using a somatic current injection (5 ms, 800–1500 pA). Fluo5-F was excited with a pE-4000 LED at 470 nm (CoolLED) at 75% intensity. Images were acquired using a Slicescope upright microscope (Scientifica), with 60×1.0 numerical aperture (NA) objective, a multiple bandpass excitation/emission filter set (LED-DA/FI/TR/Cy5A, Semrock) and ORCA-Flash4.0 CMOS camera (Hamamatsu) at 100 Hz and 2×2 pixel binning. Images were analyzed in ImageJ (NIH). For all Ca^{2+} imaging experiments and analyses, the experimenter was blind to the experimental condition.

Immunofluorescence of cultured neurons—Neuronal cultures at DIV14-16 were washed once with PBS and fixed with 4% paraformaldehyde in PBS for 10 minutes at RT.

Author Manuscript Author Manuscript Author Manuscript Author Manuscript

Cells were permeabilized in blocking solution containing 0.1% Triton X-100, 3% BSA in PBS, and incubated with primary antibodies against RIM (BD-Biosciences 610907, at 1:500 dilution for confocal microscopy, SySy 140 003, 1:500 for STED microscopy), synaptophysin (SySy 101 004, 1:500), vGAT (SySy 131 004, 1:500), Munc13-1 (SySy 126 103, 1:200), Bassoon (Enzo life sciences SAP7F407, 1:1000) and MAP-2 (Sysy 188 002, 1:1000) in blocking solution overnight at 4°C. Staining with AlexaFluor- or Oregon Green-coupled secondary antibodies (Life Technologies, 1:1000 for confocal microscopy, 1:200 for STED microscopy) was performed for 1 hr at room temperature. Coverslips were air dried at room temperature and mounted on to glass slides in mounting medium and stored at 4 °C until imaging.

STED imaging and analysis—STED microscopy was performed as described in (Wong et al., 2018). Images were acquired with a Leica SP8 Confocal/STED 3X microscope with an oil immersion 100X 1.44 NA objective. 23.3 × 23.3 μm^2 synapse-rich areas were scanned at a sampling frequency of ~10 nm/pixel. Triple-color sequential confocal scans were followed by a dual-color sequential STED scans. Alexa 633, Alexa Fluor 555 and Oregon green 488 were excited with 633 nm, 555 nm and 488 nm white light lasers respectively at 2–5% of 1.5 mW laser power in this order of sequence. During STED scanning, Oregon green 488 and Alexa Fluor 555 signals were depleted with 592 nm (75% of max power) and 660 nm (25% of max power) time-gated depletion lasers. 4-times line accumulation and 3-times frame averaging were applied during STED scanning. Identical settings were applied to all samples within an experiment. In all STED experiments, vGAT was acquired in the confocal channel. To measure protein levels at active zones, masks that contained Bassoon signal within vGAT signals were created using MATLAB. These masks were used to measure fluorescence intensity of proteins in the second STED channel. For intensity profiles, side view vGAT positive synapses (Wong et al., 2018) were selected manually, and a rectangular 0.25 μm × 1.0 μm region of interest (ROI) was placed perpendicular to the Bassoon signals in ImageJ. Profiles were aligned on peak intensity of the Bassoon signal and in each channel normalized to the peak fluorescence in control. Note that for RIM and Munc13, peak localization relative to Bassoon is not always identical, and hence the average normalized control peak intensity is slightly below 1. All quantitative analyses were performed on original images without adjustments and were done identically for all experimental conditions. For all image acquisition the experimenter was blind to the experimental condition.

Confocal microscopy—Images were acquired at an Olympus FV1000 confocal microscope using a 60×1.4 NA oil-immersion objective, and identical settings were applied to all samples within an experiment. Images were analyzed in ImageJ and MATLAB as described in (Wang et al., 2016). Synaptic levels of RIM were obtained by measuring RIM signal within synaptophysin puncta. 10 fields of view were quantified per culture per genotype. The experimenter was blind to the experimental condition of the culture.

Protein expression and purification—GST fusion proteins were expressed and purified according to standard procedures. The following proteins were produced: rat RIM1α C_2A (residues QVLPG…. WYKLQ plasmids pAJ13026, pAJ14016, pGEX-KT

Author Manuscript Author Manuscript Author Manuscript Author Manuscript

Rim1 C_2A WT, pGEX-KT Rim1 C_2A WT R834, R835E and pGEX-KT Rim1 C_2A WT K809,R811E), RIM2 C_2A (residues QFLSG…WYKLQ, pAJ13027) RIM1α C_2B domain (residues GPAQL…PCIRS, (Guan et al., 2007), pAJ13005, pAJ13014, pGEX-KT Rim1 C_2B WT and pGEX-KT Rim1 C_2B K1513,K1515E), RIM2 C_2B domain (residues GPAQL…SYSRS, pAJ13028), RIM3-C_2B (residues GPAQI…SPSCS, pAJ15025), RIM4-C_2B (residues GPAQF…CGERS, pAJ15026), rat Liprin-α3-LH1 (residues CEVMP…LEEEL, pMYW12035), rat Liprin-α3-LH2 (residues ELSNQ…ELDGS, pMYW12036), and rat Syntaxin 1a (residues 2–253 KDRTQ…SDTKK, pGEX-KT Syntaxin1). In brief, fusion proteins were expressed at 25°C in *E. coli* BL21 (DE3) for 20 h with 0.5 mM isopropyl β-D-1-thiogalactopyranoside (IPTG), except GST-Liprin-α3-LH1 and -LH2, which were expressed at 18°C for 20 h with 50 μM IPTG. For GST-pulldown experiments, cells were resuspended in PBS, and lysed using lysozyme and brief sonication. Proteins were purified using glutathione-sepharose resin in PBS and used within 5 days of purification.

For co-floatation assays, analytical ultracentrifugation and NMR spectroscopy, cells were resuspended in PBS buffer containing a protease inhibitor cocktail and lysed using an Avestin EmulsiFlex-C5 homogenizer. The RIM1α C_2A and C_2B domains were purified by the same procedure except that the RIM1α C_2B lysate was first treated with protamine sulfate (1% (w/v)) for 1 h at 4°C followed by centrifugation. The proteins were then isolated by affinity chromatography on glutathione-sepharose. Resin was washed with PBS and PBS containing 1M NaCl. Remaining nucleic acid contaminants bound to the protein were then cleared with nuclease treatment (~600 units per liter of cell culture) in 50 mM Tris (pH 8.0), 2 mM $MgCl_2$ for 2 h at room temperature with gentle rotation of the beads. The GST tag was cleaved with thrombin on the resin at room temperature for 3 h. The eluted protein was further purified by size-exclusion chromatography on a Superdex 75 16/60 column using standard buffer (20 mM MES (pH 6.0), 150 mM NaCl, 1 mM EDTA, and 0.5 mM TCEP). Uniform ^{15}N-labeling was achieved by growing the bacteria in $^{15}NH_4Cl$ as the sole nitrogen sources.

Rat Syntaxin1A (residues 2–253) in pGEX-KT was expressed by induction with 0.4 mM IPTG at an $O.D_{600}$ of 1 at 25°C for 18 hours. Cells were resuspended in resuspension buffer (RB; PBS, 1mM EDTA, 5mM DTT and protease inhibitors). Cleared lysates were applied to glutathione sepharose resin, washed with 100 ml RB, 200 ml RB + 1% Triton X-100, 200 ml RB + 1 M NaCl and 100 ml RB. The protein was then treated with nuclease for 1 hour at room temperature. The GST tag was removed by thrombin cleavage at 4°C overnight. The protein was further purified by ion exchange chromatography on a Source Q column using buffer A: 25 mM Tris pH 7.4, 1 mM TCEP and B: 25 mM Tris pH 7.4, 1M NaCl, 1mM TCEP. Source Q fractions (~38% NaCl) were frozen in liquid N_2 and stored at −80°C.

His-tagged RIM C_2A (pAJ14021 and pAJ14022) and C_2B proteins (pAJ13023, 14006, 14046, 14047, 16001–16008) were expressed using the same protocol as GST-fusion proteins. Proteins were isolated in 300 mM NaCl, 10 mM imidazole, 50 mM NaH_2PO_4 (pH 8.0) with Ni-NTA agarose and eluted from the resin in the same buffer containing 100–300 mM imidazole. After overnight dialysis to 150 mM NaCl, 25 mM HEPES (pH 8.0), aliquots

Author Manuscript Author Manuscript Author Manuscript Author Manuscript

were stored at −80°C until use. UV spectra were obtained on a Nanodrop 2000c (Thermo Fisher).

Human SNAP-25A full length in pET28A was expressed in E.coli BL21 (DE3) cells by induction with 0.4 mM IPTG at an O. D_{600} of 0.8 at 23°C for 18 hours. Cells were resuspended in 50 mM Tris pH 8, 500 mM NaCl, 4 mM Imidazole, 1% Triton X-100, protease inhibitor. Cleared lysates were applied to Ni-NTA resin, washed with 100 ml resuspension buffer containing 20 mM Imidazole and treated with nuclease at 4°C overnight. The His-tag was removed by thrombin cleavage at room temperature for 1.5 hours. The protein was further purified by size exclusion chromatography on a Superdex S75 column (GE 16/60) equilibrated with 50 mM Tris pH 8, 150 mM NaCl. Fractions were concentrated to 50 μM, frozen in liquid N_2 and stored at −80°C.

Liposome co-sedimentation—Liposome co-sedimentation was performed essentially as described in (Shin et al., 2010). Porcine brain-derived lipids were obtained from Avanti Polar lipids: L-α-phosphatidylinositol-4,5-bisphosphate ($PI(4,5)P_2$), 1,2-dioleoyl-sn-glycero-3-phospho-(1′-myo-inositol-3′,4′-bisphosphate) ($PI(3,4)P_2$), 1,2-dioleoyl-sn-glycero-3-phospho-(1′-myo-inositol-3′,5′-bisphosphate) ($PI(3,5)P_2$), 1,2-dioleoyl-sn-glycero-3-phospho-(1′-myo-inositol-3′,4′,5′-trisphosphate) ($PI(3,4,5)P_3$), L-α-phosphatidylserine (PS) and L-α-phosphatidylcholine (PC). Unless stated otherwise, the term PIP_2 refers to the $PI(4,5)P_2$ isomer. Lipids were mixed in glass tubes and dried under N_2, and resuspended in 100 mM NaCl, 25 mM HEPES (pH 8.0) and 500 mM sucrose by rigorous vortexing for 20 minutes and subsequent sonication to generate heavy liposomes. Buffer without sucrose was added to 12 ml, and liposomes were sedimented by ultracentrifugation at 150,000 × *g* for 30 min. The pellet was resuspended in buffer, and centrifuged again (20,800 × *g* 10 min). Liposome composition for each co-sedimentation experiment is indicated in the Figure legend. For binding assays, 200 μg liposomes were mixed with 10 μg protein in 1 ml buffer, and mixed for 10 minutes at 30°C while shaking at 10,00 0 RPM. Liposomes were pelleted for 10 min at 20,800 × *g at 4°C*, washed 3 times with buffer, and resuspended in 200 μl methanol:chloroform (2:1) and incubated for >30 minutes at −20°C to solubilize the lipids and precipitate the proteins. Proteins were pelleted for 15 min at 20,800 × *g* at room temperature and resuspended in 30 μL 1X SDS sample buffer. Total recovered protein was assessed by SDS-PAGE with Coomassie staining, and quantified with densitometry in ImageJ. Background protein binding to the no lipids control was subtracted from all other samples.

Liposome preparation for co-floatation—Mixtures of 1,2-dioleoyl-*sn*-glycero-3-[phospho-L-serine] (PS), 1-palmitoyl-2-oleoyl-*sn*-glycero-3-phosphocholine (PC), 1,2-dipalmitoyl-*sn*-glycero-3-phosphoethanolamine-N-(lissamine rhodamine B sulfonyl) (PE), L-α-Phosphatidylinositol (PI), L-α-Phosphatidylinositol-4-phosphate (PIP) and L-α-Phosphatidylinositol-4,5-biphosphate (PIP_2) (Avanti Polar Lipids) were prepared by mixing the lipids dissolved in chloroform in a glass test tube in the desired ratio, and chloroform was evaporated using a dry nitrogen stream. The lipids were placed in a vacuum chamber overnight to remove organic solvent. Lipid films were hydrated with reconstitution buffer (25 mM HEPES pH = 7.2, 150 mM NaCl) in an appropriate volume yielding 5 mM total

Author Manuscript Author Manuscript Author Manuscript Author Manuscript

lipid concentration. Lipids were vortexed >5 min then frozen and thawed five times. Large unilamellar vesicles were prepared by extruding the hydrated lipid solution through 0.08-μm polycarbonate membranes 23 times using an Avanti Mini-Extruder. The homogeneity of the vesicle size distribution was confirmed by dynamic light scattering on a Wyatt DynaPro instrument (Wyatt Technology, Santa Barbara, CA).

Liposome co-floatation assays—Liposomes containing PC:PE(99:1), PC:PS:PE(84:15:1), PC:PS:PE:PI (83:15:1:1), PC:PS:PE:PIP (83:15:1:1) and PC:PS:PE:PIP_2 (83:15:1:1) were mixed with the proteins with a protein/lipid (P/L) ratio of 1:200 and incubated at room temperature for 1 hr. The liposomes and bound proteins were isolated by floatation on a Histodenz density gradient (40%:35%:30%) as described (Guan et al., 2008). Samples from the top of the gradient (35 μL) were taken and analyzed by SDS-PAGE and Coomassie blue staining.

NMR spectroscopy—All NMR data were acquired at 27 °C on Varian INOVA 600 spectrometers (Varian, Palo Alto, California, USA) with RIM1 C_2 domain samples dissolved in standard buffer (20 mM MES (pH 6.0), 150 mM NaCl, 1 mM EDTA, 0.5 mM TCEP), using H_2O/D_2O 95:5 (v/v) as the solvent. All 2D ^1H-^{15}N HSQC spectra testing phospholipid binding were acquired at 100 μM and 30 μM protein concentrations for C_2A and C_2B, respectively, and dibutanoyl phosphatidylinositol 4,5-bisphosphate (diC4-PIP_2) concentrations ranging from 5 to 300 μM. Spectra testing for SNARE protein binding were performed using 20 μM ^{15}N-labeled RIM1 C_2B and 25 μM unlabeled Syntaxin or SNAP-25. The 1D ^1H-NMR spectra were acquired with samples containing 100 μM RIM1α C_2B domain and in the presence or absence of 200 μM diC4-PIP_2. All 2D NMR spectra were processed with NMRPipe (Delaglio et al., 1995) and analyzed with NMRView (Johnson and Blevins, 1994). To derive K_d values from the diC4-PIP_2 titrations, the ^{15}N chemical shifts from selected cross-peaks, which were among those that had larger diC4-PIP_2-induced chemical shift changes and were better resolved, were plotted as a function of diC4-PIP_2 concentration. The data were then fitted to a standard single-site binding model using Sigma Plot.

Analytical ultracentrifugation—All centrifugation experiments were carried out in a Beckman-Coulter Optima XL-I (Beckman-Coulter, Brea, CA) at 20 °C; a standard sedimentati on velocity protocol was used (Zhao et al., 2013). The rotor speed was 50,000 rpm and the rotor was an An50-Ti (Beckman-Coulter, Brea, CA). A280 data were analyzed in SEDFIT using the c(s) distribution model (Schuck, 2000). The distributions were normalized, integrated, and rendered in GUSSI (Brautigam, 2015), and the resulting isotherm was examined in SEDPHAT (Schuck, 2003) to estimate the K_d, assuming and fixing the values of 1.85 S for the monomer and 3.1 S for the dimer.

GST pulldowns with His-tagged proteins—To test binding of C_2B domains to Liprin sequences, 6 μg GST-Liprin-α3-LH1 or -LH2 was mixed with 15 μg His-tagged RIM C_2B WT or mutant, in 100 mM NaCl, 25 mM HEPES (pH 7.4), 0.1% Triton X-100 and 1 mM DTT. After incubation for two hours at 4°C with gentle agitation, beads were washed 5 times with 500 μl buffer, and proteins were eluted from the beads with 1× SDS sample

Author Manuscript Author Manuscript Author Manuscript Author Manuscript

buffer. Binding was determined using Coomassie-stained 15% SDS-PAGE gels. Protein intensity was measured by densitometry in ImageJ, and molar His-RIM C_2B to GST-Liprin-α3-LH was calculated by dividing both signals after correcting the raw signal for protein length.

GST pulldowns from mouse brain—To make brain lysate, brains from 6–10 week old wild type mice were homogenized in 10 ml ice cold buffer containing 100 mM NaCl, 4 mM EGTA, 25 mM HEPES (pH 7.4) and protease inhibitor cocktail (Sigma, containing AEBSP, Aprotinin, Bestatin, E-64, Leupeptin and Pepstatin A), and incubated with 1% Triton X-100 for 1 hr. The insoluble fraction was removed by ultracentrifugation at 118 K × *g* for 30 minutes. Supernatant was precleared from glutathione-binding proteins by incubation for 1 hr with 200 µl 50% glutathione-sepharose beads. Subsequently, 15 µg GST-fusion protein was mixed with 1 ml cleared brain lysate, and incubated for 1 hr at 4°C with gentle agitation. To the $+Ca^{2+}$ pulldown conditions, 5 mM $CaCl_2$ was added to obtain $[Ca^{2+}]_{free}$ of 1 mM. Beads were washed 5 times with 1 ml buffer, and proteins were eluted from the beads with 100 µl 1X SDS sample buffer. Bound proteins were identified with SDS-PAGE and western blotting.

Western blotting—SDS-PAGE gels were transferred to nitrocellulose membranes (GE Healthcare) for 6.5 hr at 4°C in buffer containing (per l) 200 ml methanol, 14 g glycine and 6 g Tris. After blocking for 1 hr at RT in TBST with 10% non-fat milk powder and 5% normal goat serum (NGS), blots were stained for 2–3 hrs at RT with primary antibodies in TBST with 5% milk and 2.5% NGS. Primary antibodies used were R809 (RIM1/2 PDZ and C_2A domains, (Schoch et al., 2002), 1:2000), HM1092 (RIM1/2 PDZ and C_2A domains, this study, 1:1000), U1130 (RIM1/2 c-terminus, (Schoch et al., 2002), 1:2000), 4396 (Liprin-α LH2 domain, (Schoch et al., 2002), 1:5000), V216 (synaptotagmin-1 cytoplasmatic domain, Südhof laboratory, 1:1000), P913 (SNAP-25, Südhof laboratory 1:2000), P939 (Synaptobrevin-2, Südhof laboratory, 1:2000), 438B (Syntaxin-1, Südhof laboratory, 1:1000), HA (Covance MMS-101P, 1:1000) and β-actin (Sigma A1978, 1:5000). After washing 5 × 5 min with TBST, blots were stained for 1 hr with horseradish peroxidase-conjugated secondary antibodies in the same solution, and blots were washed 5 × 5 min. Protein bands were visualized using enhanced chemiluminescence.

Antibody production—HM1092 RIM antibodies were raised in rabbit against a GST-fusion protein containing the PDZ domain an part of the C_2A domain of RIM1 (residues PGSAV…KVGHQ, identical to the immunogen of antibody R809, (Schoch et al., 2002), pAJ16009). The GST-fusion protein was purified as described above, and eluted from the beads with 10 mM glutathione for 3 hrs at 4°C. After overnight dialysis to PBS, the protein was snap-frozen in ethanol/dry ice and submitted to Cocalico Biologicals for immunization using standard procedures. Sera were screened using western blots on protein samples from neuronal RIM1/2 control and RIM1/2 cDKO cultures. The serum with highest specific immunoreactivity (HM1092) for RIM was selected for use.

Author Manuscript Author Manuscript Author Manuscript Author Manuscript

Quantification and statistical analysis

For electrophysiological and STED experiments, statistical differences were assessed using a one-way Kruskal-Wallis ANOVA with tukey-kramer correction for multiple testing, comparing against the cDKO condition. For PPR, a two-way ANOVA with tukey-kramer correction for multiple testing was used, testing genotype against cDKO. P values reported for one- and two-way ANOVAs are derived from the post-hoc test as reported in each figure legend. For lipid co-sedimentation in Figures 3 and S3 and GST-pulldowns in Figure 6, a Student's t-test was used. In all figures, * indicates $p < 0.05$, ** $p < 0.01$, and *** $p < 0.001$. No tests were used to estimate sample size. Except for NMR spectra and co-floatation assays, all experiments were performed at least 3 times to ensure reproducibility. The statistical tests used, the definition of n and the number of observations per experimental condition are specified in the figure legends. In all experiments, data is represented as mean ± standard error of the mean (SEM).

Supplementary Material

Refer to Web version on PubMed Central for supplementary material.

Acknowledgments

We thank Lydia Bickford and Jennifer Jiexin Wang for technical support, Hajnalka Nyitrai for help with antibody production, Dr. Thomas Südhof for antibodies, and Dr. Jonathan Cohen and members of the Kaeser laboratory for comments on the manuscript. This work was supported by grants from the NIH (R01NS083898 and R01MH113349 to PSK; R35 NS097333 to JR), the Lefler Foundation (to AdJ), the NWO (Rubicon Fellowship 825.12.028 to AdJ), the Harvard Brain Initiative (to PSK) and the Welch Foundation (I-1304 to JR). We also acknowledge the Neurobiology Imaging Facility (supported by a P30 Core Center Grant NS072030) and the Harvard Neurodiscovery Imaging Center.

References

Andrews-Zwilling YS, Kawabe H, Reim K, Varoqueaux F, Brose N. Binding to Rab3A-interacting molecule RIM regulates the presynaptic recruitment of Munc13-1 and ubMunc13-2. J Biol Chem. 2006; 281:19720–19731. [PubMed: 16704978]

Aoyagi K, Sugaya T, Umeda M, Yamamoto S, Terakawa S, Takahashi M. The activation of exocytotic sites by the formation of phosphatidylinositol 4,5-bisphosphate microdomains at syntaxin clusters. J Biol Chem. 2005; 280:17346–17352. [PubMed: 15741173]

Augustin I, Rosenmund C, Südhof TC, Brose N. Munc13-1 is essential for fusion competence of glutamatergic synaptic vesicles. Nature. 1999; 400:457–461. [PubMed: 10440375]

Bai J, Tucker WC, Chapman ER. PIP2 increases the speed of response of synaptotagmin and steers its membrane-penetration activity toward the plasma membrane. Nat Struct Mol Biol. 2004; 11:36–44. [PubMed: 14718921]

van den Bogaart G, Meyenberg K, Risselada HJ, Amin H, Willig KI, Hubrich BE, Dier M, Hell SW, Grubmüller H, Diederichsen U, et al. Membrane protein sequestering by ionic protein–lipid interactions. Nature. 2011; 479:552–555. [PubMed: 22020284]

Van den Bogaart G, Meyenberg K, Diederichsen U, Jahn R. Phosphatidylinositol 4,5-bisphosphate increases Ca2+ affinity of synaptotagmin-1 by 40-fold. J Biol Chem. 2012; 287:16447–16453. [PubMed: 22447935]

Brautigam CA. Calculations and Publication-Quality Illustrations for Analytical Ultracentrifugation Data. Methods Enzymol. 2015; 562:109–133. [PubMed: 26412649]

Camacho M, Basu J, Trimbuch T, Chang S, Pulido-Lozano C, Chang SS, Duluvova I, Abo-Rady M, Rizo J, Rosenmund C. Heterodimerization of Munc13 C2A domain with RIM regulates synaptic vesicle docking and priming. Nat Commun. 2017; 8:15293. [PubMed: 28489077]

Author Manuscript Author Manuscript Author Manuscript Author Manuscript

Coppola T, Magnin-Lüthi S, Perret-Menoud V, Gattesco S, Schiavo G, Regazzi R. Direct Interaction of the Rab3 Effector RIM with Ca2+ Channels, SNAP-25, and Synaptotagmin. J Biol Chem. 2001; 276:32756–32762. [PubMed: 11438518]

Corbalan-Garcia S, Gómez-Fernández JC. Signaling through C2 domains: More than one lipid target. Biochim Biophys Acta - Biomembr. 2014; 1838:1536–1547.

Coudevylle N, Montaville P, Leonov A, Zweckstetter M, Becker S. Structural determinants for Ca2+ and phosphatidylinositol 4,5-bisphosphate binding by the C2A domain of rabphilin-3A. J Biol Chem. 2008; 283:35918–35928. [PubMed: 18945677]

Dai H, Tomchick DR, García J, Südhof TC, Machius M, Rizo J. Crystal structure of the RIM2 C2A-domain at 1.4 Å resolution. Biochemistry. 2005; 44:13533–13542. [PubMed: 16216076]

Delaglio F, Grzesiek S, Vuister GW, Zhu G, Pfeifer J, Bax A. NMRPipe: A multidimensional spectral processing system based on UNIX pipes. J Biomol NMR. 1995; 6:277–293. [PubMed: 8520220]

Deng L, Kaeser PS, Xu W, Südhof TC. RIM proteins activate vesicle priming by reversing autoinhibitory homodimerization of munc13. Neuron. 2011; 69:317–331. [PubMed: 21262469]

Eggermann E, Bucurenciu I, Goswami SP, Jonas P. Nanodomain coupling between Ca^{2+} channels and sensors of exocytosis at fast mammalian synapses. Nat Rev Neurosci. 2012; 13:7–21.

Giordano F, Saheki Y, Idevall-Hagren O, Colombo SF, Pirruccello M, Milosevic I, Gracheva EO, Bagriantsev SN, Borgese N, De Camilli P. PI(4,5)P2-Dependent and Ca2+-Regulated ER-PM interactions mediated by the extended synaptotagmins. Cell. 2013; 153:1494–1509. [PubMed: 23791178]

Groffen AJ, Martens S, Arazola RD, Cornelisse LN, Lozovaya N, de Jong APH, Goriounova NA, Habets RLP, Takai Y, Borst JG, et al. Doc2b Is a High-Affinity Ca2+ Sensor for Spontaneous Neurotransmitter Release. Science. 2010; 327:1614–1618. [PubMed: 20150444]

Guan R, Dai H, Tomchick DR, Dulubova I, Machius M, Sudhof TC, Rizo J. Crystal Structure of the RIM1a C2B Domain at 1.7 Å Resolution. Biochemistry. 2007; 46:8988–8998. [PubMed: 17630786]

Guan R, Dai H, Rizo J. Binding of the Munc13-1 MUN Domain to Membrane-Anchored SNARE complexes. Biochem. 2008; 47:1474–1481. [PubMed: 18201107]

Guerrero-Valero M, Ferrer-Orta C, Querol-Audi J, Marin-Vicente C, Fita I, Gomez-Fernandez JC, Verdaguer N, Corbalan-Garcia S. Structural and mechanistic insights into the association of PKC-C2 domain to PtdIns(4,5)P2. Proc Natl Acad Sci. 2009; 106:6603–6607. [PubMed: 19346474]

Han Y, Kaeser PS, Südhof TC, Schneggenburger R. RIM determines Ca2+ channel density and vesicle docking at the presynaptic active zone. Neuron. 2011; 69:304–316. [PubMed: 21262468]

Hay JC, Fisette PL, Jenkins GH, Fukami K, Takenawa T, Anderson RA, Martin TF. ATP-dependent inositide phosphorylation required for Ca2+-activated secretion. Nature. 1995; 374:173–177. [PubMed: 7877690]

Hibino H, Pironkova R, Onwumere O, Vologodskaia M, Hudspeth aJ, Lesage F. RIM - binding proteins (RBPs) couple Rab3 - interacting molecules (RIMs) to voltage - gated Ca2+ channels. Neuron. 2002; 34:411–423. [PubMed: 11988172]

Honigmann A, van den Bogaart G, Iraheta E, Risselada HJ, Milovanovic D, Mueller V, Müllar S, Diederichsen U, Fasshauer D, Grubmüller H, et al. Phosphatidylinositol 4,5-bisphosphate clusters act as molecular beacons for vesicle recruitment. Nat Struct Mol Biol. 2013; 20:679–686. [PubMed: 23665582]

Imig C, Min SW, Krinner S, Arancillo M, Rosenmund C, Südhof TC, Rhee JS, Brose N, Cooper BH. The Morphological and Molecular Nature of Synaptic Vesicle Priming at Presynaptic Active Zones. Neuron. 2014; 84:416–431. [PubMed: 25374362]

Jahn R, Fasshauer D. Molecular machines governing exocytosis of synaptic vesicles. Nature. 2012; 490:201–207. [PubMed: 23060190]

Johnson BA, Blevins RA. NMRVIEW: a computer program for the visualization and analysis of NMR data. J Biomol NMR. 1994; 4:603–614. [PubMed: 22911360]

Johnson S, Halford S, Morris AG, Patel RJ, Wilkie SE, Hardcastle AJ, Moore AT, Zhang K, Hunt DM. Genomic organisation and alternative splicing of human RIM1, a gene implicated in autosomal dominant cone-rod dystrophy (CORD7). Genomics. 2003; 81:304–314. [PubMed: 12659814]

Author Manuscript Author Manuscript Author Manuscript Author Manuscript

Kaeser PS, Regehr WG. The readily releasable pool of synaptic vesicles. Curr Opin Neurobiol. 2017; 43:63–70. [PubMed: 28103533]

Kaeser PS, Kwon HB, Chiu CQ, Deng L, Castillo PE, Sudhof TC. RIM1 and RIM1 Are Synthesized from Distinct Promoters of the RIM1 Gene to Mediate Differential But Overlapping Synaptic Functions. J Neurosci. 2008; 28:13435–13447. [PubMed: 19074017]

Kaeser PS, Deng L, Wang Y, Dulubova I, Liu X, Rizo J, Südhof TC. RIM proteins tether Ca2+ channels to presynaptic active zones via a direct PDZ-domain interaction. Cell. 2011; 144:282–295. [PubMed: 21241895]

Kaeser PS, Deng L, Fan M, Südhof TC. RIM genes differentially contribute to organizing presynaptic release sites. Proc Natl Acad Sci U S A. 2012; 109:11830–11835. [PubMed: 22753485]

Kiyonaka S, Wakamori M, Miki T, Uriu Y, Nonaka M, Bito H, Beedle AM, Mori E, Hara Y, De Waard M, et al. RIM1 confers sustained activity and neurotransmitter vesicle anchoring to presynaptic Ca2+ channels. Nat Neurosci. 2007; 10:691–701. [PubMed: 17496890]

Koch M, Holt M. Coupling exo- and endocytosis: An essential role for PIP 2 at the synapse. Biochim Biophys Acta - Mol Cell Biol Lipids. 2012; 1821:1114–1132.

Koushika SP, Richmond JE, Hadwiger G, Weimer RM, Jorgensen EM, Nonet ML. A post-docking role for active zone protein Rim. Nat Neurosci. 2001; 4:997–1005. [PubMed: 11559854]

Lauwers E, Goodchild R, Verstreken P. Membrane Lipids in Presynaptic Function and Disease. Neuron. 2016; 90:11–25. [PubMed: 27054615]

Laux T, Fukami K, Thelen M, Golub T, Frey D, Caroni P. Rafts, and Regulate Cell Cortex Actin Dynamics through a Common Mechanism. Cell. 2000; 149:1455–1471.

Li L, Shin OH, Rhee JS, Araç D, Rah JC, Rizo J, Südhof T, Rosenmund C. Phosphatidylinositol phosphates as co-activators of Ca2+ binding to C2 domains of synaptotagmin 1. J Biol Chem. 2006; 281:15845–15852. [PubMed: 16595652]

Liu KS, Siebert M, Mertel S, Knoche E, Wegener S, Wichmann C, Matkovic T, Muhammad K, Depner H, Mettke C, et al. RIM-Binding Protein, a Central Part of the Active Zone, Is Essential for Neurotransmitter Release. Science. 2011; 334:1565–1569. [PubMed: 22174254]

Maschi D, Klyachko VA. Spatiotemporal Regulation of Synaptic Vesicle Fusion Sites in Central Synapses. Neuron. 2017; 94:65–73e3. [PubMed: 28343869]

Maximov A, Pang ZP, Tervo DGR, Südhof TC. Monitoring synaptic transmission in primary neuronal cultures using local extracellular stimulation. J Neurosci Methods. 2007; 161:75–87. [PubMed: 17118459]

Milosevic I, Sorensen J, Lang T, Krauss M, Nagy G, Hauke V, Jahn R, Neher E. Plasmalemmal Phosphatidylinositol-4,5-Bisphosphate Level Regulates the Releasable Vesicle Pool Size in Chromaffin Cells. J Neurosci. 2005; 25:2557–2565. [PubMed: 15758165]

Montaville P, Coudevylle N, Radhakrishnan A, Leonov A, Zweckstetter M, Becker S. The PIP2 binding mode of the C2 domains of rabphilin-3A. Protein Sci. 2008; 17:1025–1034. [PubMed: 18434502]

Muller M, Liu KSY, Sigrist SJ, Davis GW. RIM Controls Homeostatic Plasticity through Modulation of the Readily-Releasable Vesicle Pool. J Neurosci. 2012; 32:16574–16585. [PubMed: 23175813]

Di Paolo G, De Camilli P. Phosphoinositides in cell regulation and membrane dynamics. Nature. 2006; 443:651–657. [PubMed: 17035995]

Di Paolo G, Moskowitz HS, Gipson K, Wenk MR, Voronov S, Obayashi M, Flavell R, Fitzsimonds RM, Ryan Ta, De Camilli P. Impaired PtdIns(4,5)P2 synthesis in nerve terminals produces defects in synaptic vesicle trafficking. Nature. 2004; 431:415–422. [PubMed: 15386003]

Rosenmund C, Stevens CF. Definition of the readily releasable pool of vesicles at hippocampal synapses. Neuron. 1996; 16:1197–1207. [PubMed: 8663996]

Schoch S, Castillo PE, Jo T, Mukherjee K, Geppert M, Wang Y, Schmitz F, Malenka RC, Südhof TC. RIM1α forms a protein scaffold for regulating neurotransmitter release at the active zone. Nature. 2002; 415:321–326. [PubMed: 11797009]

Schuck P. Size-Distribution Analysis of Macromolecules by Sedimentation Velocity Ultracentrifugation and Lamm Equation Modeling. Biophys J. 2000; 78:1606–1619. [PubMed: 10692345]

Author Manuscript Author Manuscript Author Manuscript Author Manuscript

Schuck P. On the analysis of protein self-association by sedimentation velocity analytical ultracentrifugation. Anal Biochem. 2003; 320:104–124. [PubMed: 12895474]

Shin OH, Lu J, Rhee JS, Tomchick DR, Pang ZP, Wojcik SM, Camacho-Perez M, Brose N, Machius M, Rizo J, et al. Munc13 C2B domain is an activity-dependent Ca2+ regulator of synaptic exocytosis. Nat Struct Mol Biol. 2010; 17:280–288. [PubMed: 20154707]

Südhof TC. The presynaptic active zone. Neuron. 2012; 75:11–25. [PubMed: 22794257]

Südhof TC. Neurotransmitter release: The last millisecond in the life of a synaptic vesicle. Neuron. 2013; 80:675–690. [PubMed: 24183019]

Suh BC, Leal K, Hille B. Modulation of high-voltage activated Ca2+ channels by membrane phosphatidylinositol 4,5-bisphosphate. Neuron. 2010; 67:224–238. [PubMed: 20670831]

Tang AH, Chen H, Li TP, Metzbower SR, MacGillavry HD, Blanpied TA. A trans-synaptic nanocolumn aligns neurotransmitter release to receptors. Nature. 2016; 536:210–214. [PubMed: 27462810]

Ubach J, Lao Y, Fernandez I, Arac D, Südhof TC, Rizo J. The C2B domain of synaptotagmin I is a Ca2+-binding module. Biochemistry. 2001; 40:5854–5860. [PubMed: 11352720]

Uriu Y, Kiyonaka S, Miki T, Yagi M, Akiyama S, Mori E, Nakao A, Beedle AM, Campbell KP, Wakamori M, et al. Rab3-interacting molecule γ isoforms lacking the rab3-binding domain induce long lasting currents but block neurotransmitter vesicle anchoring in voltage-dependent P/Q-type Ca2+ channels. J Biol Chem. 2010; 285:21750–21767. [PubMed: 20452978]

Wang Y, Südhof TC. Genomic definition of RIM proteins: Evolutionary amplification of a family of synaptic regulatory proteins. Genomics. 2003; 81:126–137. [PubMed: 12620390]

Wang SSH, Held RG, Wong MY, Liu C, Karakhanyan A, Kaeser PS. Fusion Competent Synaptic Vesicles Persist upon Active Zone Disruption and Loss of Vesicle Docking. Neuron. 2016; 91:777–791. [PubMed: 27537483]

Wickner W. Membrane fusion: five lipids, four SNAREs, three chaperones, two nucleotides, and a Rab, all dancing in a ring on yeast vacuoles. Annu Rev Cell Dev Biol. 2010; 26:115–136. [PubMed: 20521906]

Wong MY, Liu C, Wang SSH, Roquas ACF, Fowler S, Kaeser PS. Liprin-α 3 controls vesicle docking and exocytosis at the active zone of hippocampal synapses. Proc Natl Acad Sci. 2018; ePub ahead of print (2/8/2018). doi: 10.1073/pnas.1719012115

Yasuda T, Shibasaki T, Minami K, Takahashi H, Mizoguchi A, Uriu Y, Numata T, Mori Y, Miyazaki JI, Miki T, et al. Rim2a determines docking and priming states in insulin granule exocytosis. Cell Metab. 2010; 12:117–129. [PubMed: 20674857]

Zhao H, Brautigam CA, Ghirlando R, Schuck P. Overview of current methods in sedimentation velocity and sedimentation equilibrium analytical ultracentrifugation. Curr Protoc Protein Sci. 2013:1–49.

Zucker RS, Regehr WG. Short-Term Synaptic Plasticity. Annu Rev Physiol. 2002; 64:355–405. [PubMed: 11826273]

Author Manuscript Author Manuscript Author Manuscript Author Manuscript

Highlights

- RIM C_2B controls synaptic vesicle fusion downstream of priming and Ca^{2+} influx
- C_2B domains bind to PIP_2 and PIP_2 binding is required for RIM's role in release
- C_2B domains need to be tethered to other RIM domains for mediating vesicle fusion
- RIM C_2B domains have additional functions for enhancing release probability

Author Manuscript Author Manuscript Author Manuscript Author Manuscript

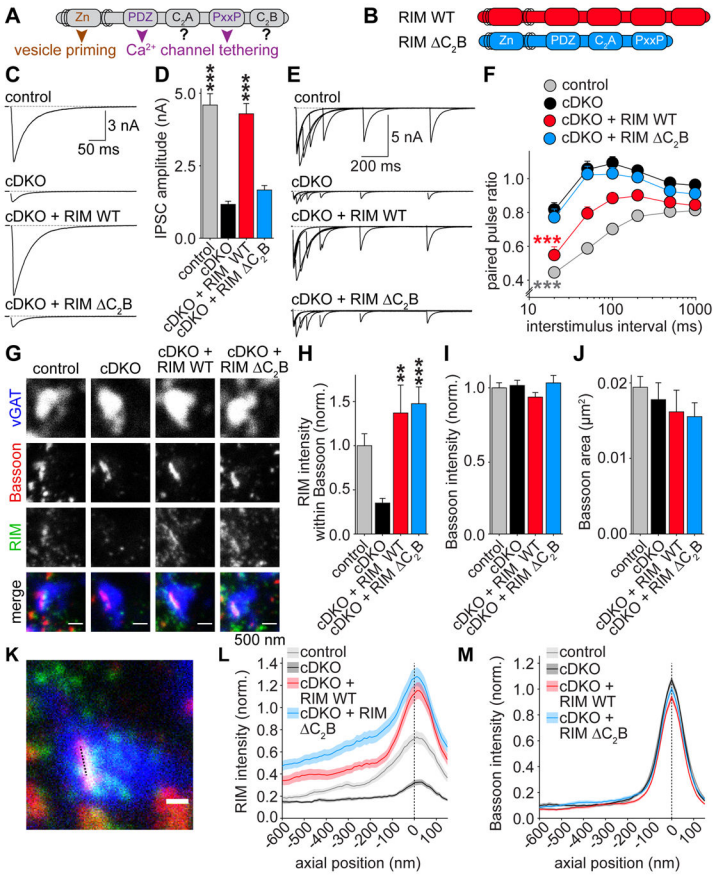

Figure 1. The RIM1 C_2B domain is crucial for synaptic vesicle release

(A) Domain structure of RIM1α (Zn: zinc finger domain with surrounding α-helical regions, PxxP: proline-rich region) and key RIM functions that are assigned to specific domains.

(B) Overview of rescue proteins.

(C, D) Example traces (C) and quantification of average amplitudes (D) of single evoked IPSCs in cultured hippocampal neurons. cDKO neurons are neurons from RIM1/2 conditional knockout mice infected with a lentivirus expressing Cre recombinase, and rescue proteins were expressed from a second, independent lentivirus. Control neurons are neurons from the same culture infected with a virus expressing truncated, inactive cre. Control n = 6 independent cultures/30 cells, cDKO 6/30, cDKO + RIM WT 6/31, cDKO + RIM ΔC_2B 6/32.

(E, F) Example traces (E) and average IPSC paired pulse ratios (F) at various interstimulus intervals. Control n = 4 independent cultures/21 cells, cDKO 4/18, cDKO + RIM WT 4/21, cDKO + RIM ΔC_2B 4/21. *** $p < 0.001$ genotype vs cDKO by two-way ANOVA.

(G–J) Example images (G) and quantification (H–J) of synapses using STED microscopy. Average RIM intensity within Bassoon objects (H), average Bassoon intensity within Bassoon objects (I), and average surface area of Bassoon objects (J) are shown. Control n = 3 independent cultures/10 fields of view (23.5 μm x 23.5 μm, typically containing 100 – 300 Bassoon objects per field of view), cDKO 3/7, cDKO + RIM WT 3/8, cDKO + RIM ΔC_2B 3/11.

Author Manuscript Author Manuscript Author Manuscript Author Manuscript

(K–M) Schematic representation (K) and intensity profile analysis (L, M) of side view synapses. Shaded area represents the ROI, the dotted line indicates distance = 0 nm centered to the peak of Bassoon labeling. Average intensity profiles of RIM (L) and Bassoon (M) are shown. Data are shown as mean (solid line) ± SEM (shaded area). Control n = 3 independent cultures/67 ROIs, cDKO 3/72, cDKO + RIM WT 3/83, cDKO + RIM ΔC_2B 3/87.
All data are mean ± SEM, * $p < 0.05$, ** $p < 0.01$, *** $p < 0.001$ analyzed by one-way ANOVA (Kruskal Wallis; D, H–J) unless otherwise noted, all comparisons to cDKO. For assessment of synaptic transmission upon expression of RIM WT and RIM ΔC_2B in wild type neurons and analysis of RIM ΔC_2A rescue, see Figure S1, for STED overview images see Figure S2A.

Author Manuscript Author Manuscript Author Manuscript Author Manuscript

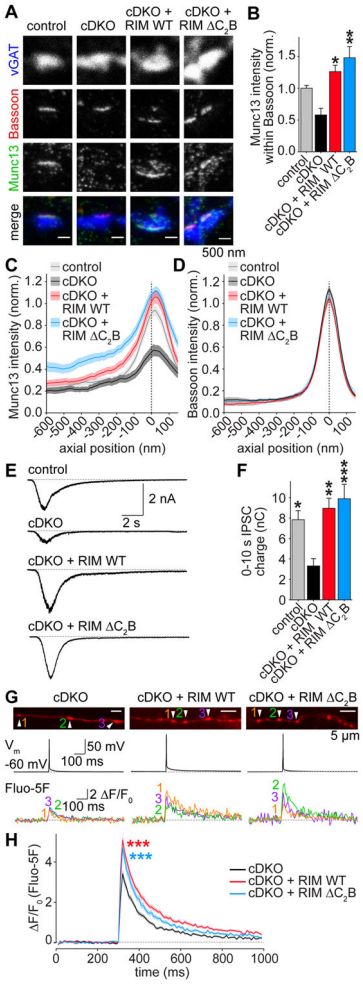

Figure 2. RIM1 C_2B domains are dispensable for the functions of RIM in Munc13 recruitment, vesicle priming and Ca^{2+} influx

(A, B) Example images (A) and average Munc13 intensity (B) of synapses in STED microscopy. Control n = 3 independent cultures/7 fields of view, cDKO 3/6, cDKO + RIM WT 3/6, cDKO + RIM ΔC_2B 3/6.

(C, D) Intensity profile for Munc13 (C) and Bassoon (D) in side view synapses. Control n = 3 independent cultures/60 ROIs, cDKO 3/53, cDKO + RIM WT 3/64, cDKO + RIM ΔC_2B 3/66.

(E, F) Example traces (E) and quantification of IPSC charge (F) integrated over 10 s, induced by a focal 10 s puff of hyperosmolar sucrose (500 mM) as a measurement of the RRP. Control n = 3 independent cultures/13 cells, cDKO 3/15, cDKO + RIM WT 3/13, cDKO + RIM ΔC_2B 3/13.

(G, H) Example boutons (G) and quantification (H) of presynaptic Ca^{2+} imaging. Individual cells were filled with Alexa 647 and the Ca^{2+} indicator Fluo-5F through a patch pipette. In G, images of Alexa 647 fluorescence in axons (top), the somatic membrane potentials (middle) and Fluo-5F fluorescence traces of individual boutons during a single action potential (bottom) in response to a brief somatic current injection are shown. Arrowheads in Alexa 647 images indicate boutons from which Fluo-5F signals at the bottom were obtained.

Author Manuscript Author Manuscript Author Manuscript Author Manuscript

H shows the average Fluo-5F $\Delta F/F_0$ during a single action potential. cDKO n = 3 independent cultures/8 cells/153 boutons, cDKO + RIM WT 3/8/160, cDKO + RIM ΔC_2B 3/8/93. *** $p < 0.001$ genotype vs cDKO by 2-way ANOVA, for first 6 frames after stimulation.

All data are mean ± SEM, *$p < 0.05$, ** $p < 0.01$, *** $p < 0.001$ vs cDKO analyzed by one-way ANOVA (Kruskal Wallis; B,F) unless otherwise noted, all comparisons to cDKO. For overview STED images and quantification of Bassoon signals, see Figures S2B–S2D.

Author Manuscript Author Manuscript Author Manuscript Author Manuscript

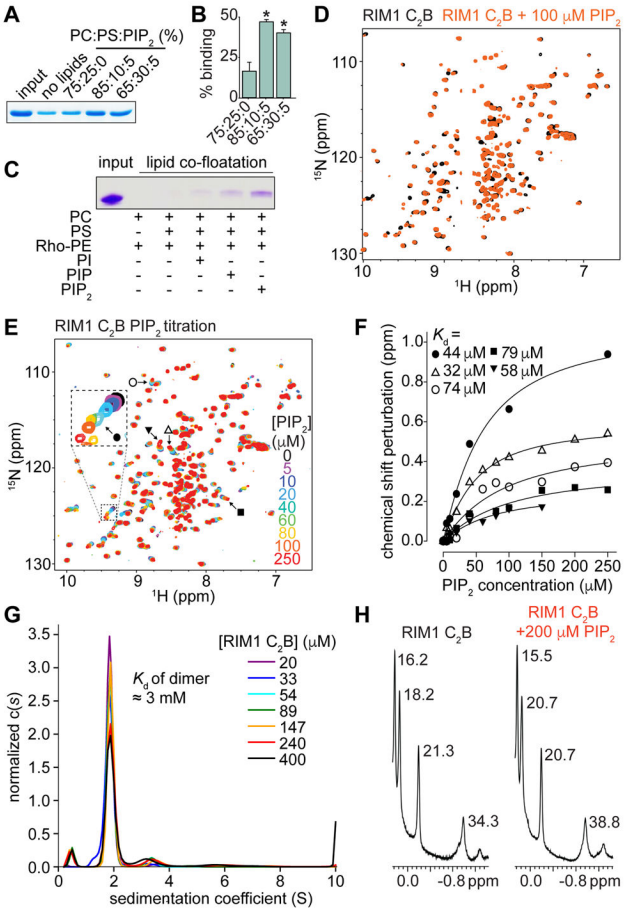

Figure 3. RIM1 C_2B domains bind specifically to the phospholipid PIP_2

(A, B) Example Coomassie stained SDS-PAGE gel (A) and average C_2B domain content in the pellet (B) of a lipid co-sedimentation experiment using heavy liposomes of various compositions and purified His-C_2B domains. PC: phosphatidylcholine, PS: phosphatidylserine. Averages ± SEM are obtained from 3 independent experiments. Statistical significance was assessed by Students *t*-test, with * $p < 0.05$ vs the 75:25:0 condition.

(C) Image of a Coomassie stained SDS-PAGE of a lipid co-floatation assay to test for PIP_2 specificity of lipid-C_2B binding. The assay was performed with purified RIM1 C_2B and various liposome compositions, as indicated.

(D) Analysis of PIP_2 binding to RIM1 C_2B using NMR spectroscopy. Superposition of ^1H-^{15}N HSQC spectra of ^{15}N-labeled RIM1 C_2B alone (black contours) and in the presence of 100 μM diC4-PIP_2 (orange contours), a water soluble PIP_2 analogue.

(E) Superposition of ^1H-^{15} N HSQC spectra of RIM1 C_2B acquired in the presence of different diC4-PIP_2 concentrations as indicated by the color code. Symbols indicate cross-peak shifts for which the dissociation constants (K_d) in panel F were calculated.

(F) Analysis of the binding affinity of PIP_2 to ^{15}N-labeled RIM1 C_2B using NMR spectroscopy. Plots of ^{15}N chemical shift perturbations (corresponding to labels in panel E) as a function of diC4-PIP_2 concentration for selected cross-peaks. The data for each cross-peak were fitted with a standard single-site binding model, yielding the K_d per cross-peak.

Author Manuscript Author Manuscript Author Manuscript Author Manuscript

(G) Analytical ultracentrifugation of RIM1 C_2B at various concentrations. The $c(s)$ distributions shown were normalized to the total signal in each distribution. The K_d of the dimer is indicated in the figure.

(H) Expansions showing the well-resolved methyl resonances of 1D ^{1}H-NMR spectra of RIM1 C_2B alone (left) and in the presence of 200 μM diC4-PIP_2 (right). The line widths (in Hz) are indicated next to each resonance and are comparable in the two spectra.

For experiments assessing PIP_2 binding of RIM1 C_2A, see Figure S3.

Author Manuscript Author Manuscript Author Manuscript Author Manuscript

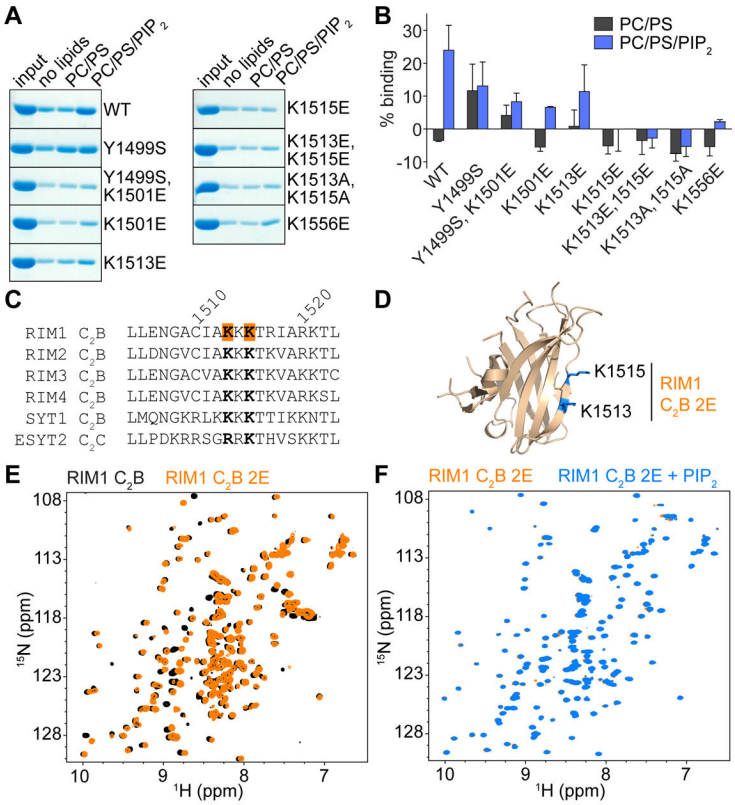

Figure 4. Mutations in the polybasic sequence of RIM1 C_2B abolish PIP_2 binding

(A, B) Example gels (A) and quantification (B) of liposome co-sedimentation assays using His-C_2B domains. Binding was quantified as percent of total input, and the signal in the no lipids sample was set to 0% for normalization. Data shown as mean ± SEM from 3 independent experiments. Liposome composition (PC:PS:PIP_2): PC/PS: 65:35:0, PC/PS/PIP_2 65:30:5.

(C) Sequence alignment (also see Figure S3G) of the polybasic sequence of the C_2B domains of rat RIM1 (Uniprot ID Q9JIR4), RIM2 (Q9JIS1), RIM3 (Q9JIR3), RIM4 (Q8CIX1), synaptotagmin-1 (SYT1, P21707) and human extended synaptotagmin 2 (ESYT2, A0FGR8). The lysine residues mutated in RIM1 C_2B 2E are highlighted in orange. Conservation of mutated lysines is shown in bold. Numbers on top indicate residue positions in RIM1.

(D) Ribbon diagram of the RIM1 C_2B domain showing the locations of the mutated residues (PDB: 2Q3X, (Guan et al., 2007)).

(E) Superposition of ^1H-^{15}N HSQC spectra of ^{15}N-labeled RIM1 C_2B WT (black contours) and RIM1 C_2B 2E (orange contours) domains.

(F) Analysis of PIP_2 binding to ^{15}N-labeled RIM1 C_2B 2E using NMR spectroscopy. Superposition of ^1H-^{15}N HSQC spectra of RIM1 C_2B 2E alone (orange contours) and RIM1 C_2B 2E in the presence of 100 μM diC4-PIP_2 (blue contours).

For mutational analyses of C_2A-PIP_2 binding and of binding of RIM C_2 domains to PIP_3 and various PIP_2 isomers, see Figure S4.

Author Manuscript Author Manuscript Author Manuscript Author Manuscript

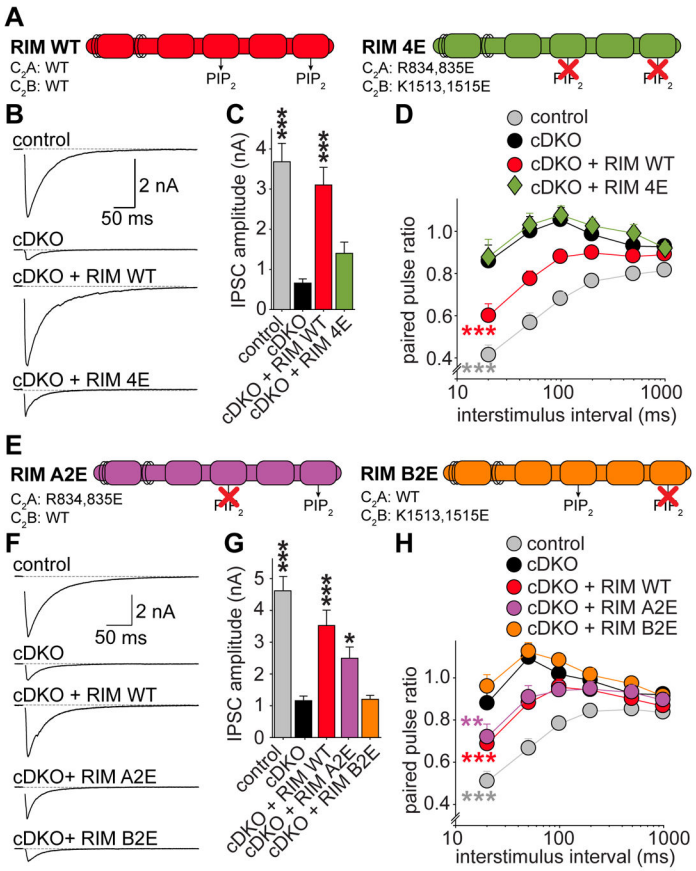

Figure 5. The PIP_2-binding interface of C_2B controls synaptic vesicle release

(A) Overview of rescue proteins.

(B, C) Example traces (B) and quantification of average amplitudes (C) of single evoked IPSCs. Control n = 8 independent cultures/34 cells, cDKO 8/32, cDKO + RIM WT 8/39, cDKO + RIM 4E 8/38.

(D) IPSC paired pulse ratios at various interstimulus intervals. Control n = 3 independent cultures/11 cells, cDKO 3/12, cDKO + RIM WT 3/14, cDKO + RIM 4E 3/14.

(E–H) Identical to A–D, but for mutations in only the C_2A (A2E) or C_2B (B2E) domains. Control n = 4 independent cultures/15 cells, cDKO 4/16, cDKO + RIM WT 4/17, cDKO + RIM A2E 4/19, cDKO + RIM B2E 4/19.

All data shown as mean ± SEM, *p < 0.05, ** p < 0.01, *** p < 0.001 for IPSC amplitudes analyzed by one-way ANOVA (Kruskal Wallis; C, G), for PPRs analyzed by two-way ANOVA (D, H), all comparisons to cDKO. For expression analysis of rescue proteins, RRP measurements, example traces for PPRs and analyses of stimulation trains, see Figure S5.

Author Manuscript Author Manuscript Author Manuscript Author Manuscript

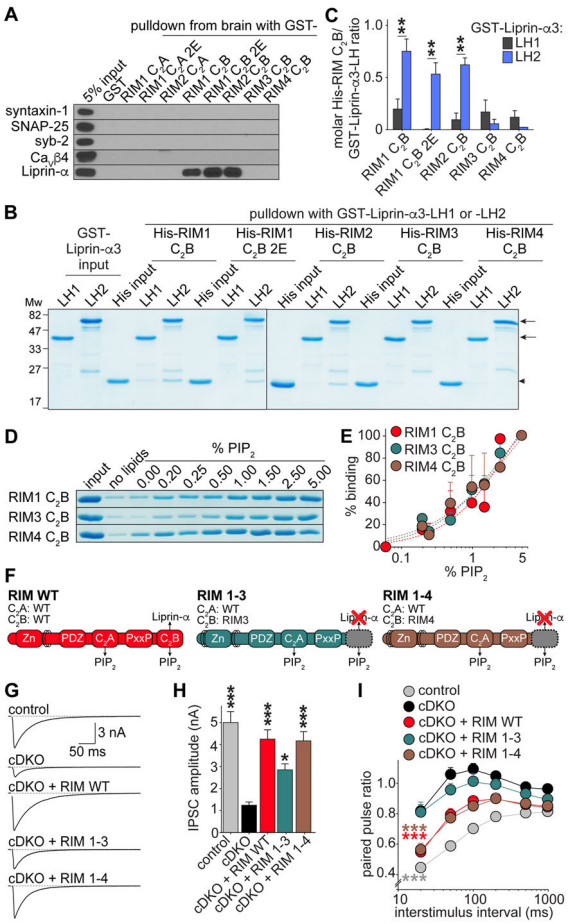

Figure 6. PIP_2- but not Liprin-α-binding of RIM C_2B is required for rescue

(A) Example images of western blots of GST affinity purifications to test for binding of RIM C_2 domains to syntaxin-1, SNAP-25, synaptobrevin/VAMP-2 (syb-2), $Ca_V\beta4$ subunits and Liprin-α from mouse brain lysate. Each experiment was performed in at least 3 independent repeats.

(B, C) Representative gels (B) and quantification (C) of affinity binding assays with GST-Liprin-α3-LH1 -LH2 on beads and His-tagged RIM C_2B variants in solution. Arrows in B indicate GST- Liprin-α3-LH1 and -LH2 bands; arrowheads indicate His-RIM C_2B band. Average molar His-RIM C_2B/GST-Liprin-α3-LH ratio was obtained from 3 independent replicates.

(D, E) Representative gels (D) and quantification (E, average of 3 independent repeats) of lipid co-sedimentation of RIM1, RIM3 and RIM4 His-C_2B domains with heavy liposomes with increasing content of PIP_2. Liposome composition (PC:PS:PIP_2): 0% PIP_2 (65:35:0), up to 5% PIP_2 (65:30:5). Dotted line in E represents a Hill-fit through the data points.

(F) Overview of rescue proteins.

(G, H) Example traces (G) and quantification of average amplitudes (H) of single evoked IPSCs. Control n = 4 independent cultures/21 cells, cDKO 4/21, cDKO + RIM WT 4/22, cDKO + RIM 1–3 3/16, cDKO + RIM1-4 4/21.

(I) IPSC paired pulse ratios at various interstimulus intervals. Number of observations as in H.

Author Manuscript Author Manuscript Author Manuscript Author Manuscript

All data shown as mean ± SEM, * $p < 0.05$, ** $p < 0.01$, *** $p < 0.001$ for protein interactions by Students t-test (C), for IPSC amplitudes analyzed by one-way ANOVA (Kruskal Wallis; H), for PPRs analyzed by two-way ANOVA (I); all comparisons to cDKO. For additional analyses of RIM C_2B-SNARE interactions and synaptotagmin-1 binding, see Figure S6, for assessment of rescue RIM expression, example traces of PPRs, and a rescue experiment in which the RIM C_2B domain was replaced by the Extended synaptotagmin 2 C_2C domain, see Figure S7A–S7J.

Author Manuscript Author Manuscript Author Manuscript Author Manuscript

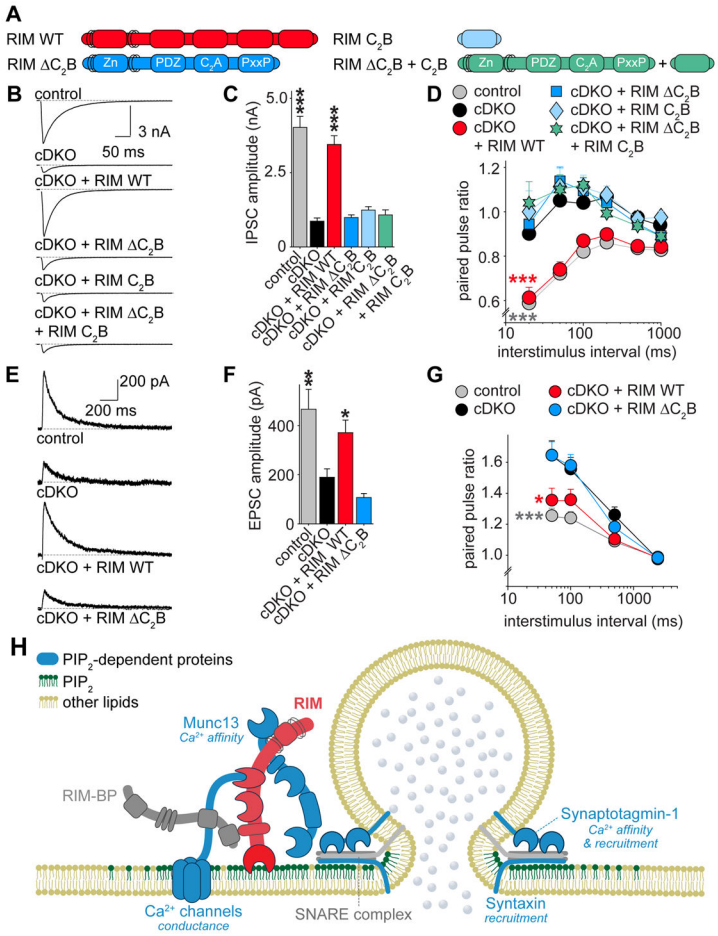

Figure 7. Tethering of RIM C_2B to N-terminal RIM domains is essential for rescue

(A) Overview of rescue proteins.

(B, C) Example traces (B) and quantification of average amplitudes (C) of single evoked IPSCs. Control n = 3 independent cultures/16 cells, cDKO 3/15, cDKO + RIM WT 3/16, cDKO + RIM Δ C_2B 3/15, cDKO + RIM C_2B 3/15, cDKO + RIM ΔC_2B + RIM C_2B 3/15.

(D) Quantification of IPSC paired pulse ratios at various interstimulus intervals. Number of observations as in C.

(E, F) Example traces (E) and quantification of average amplitudes (F) of single evoked NMDA receptor EPSCs in cultured hippocampal neurons. Control n = 4 independent cultures/18 cells, cDKO 4/19, cDKO + RIM WT 4/20, cDKO + RIM ΔC_2B 4/19.

(G) Quantification of EPSC paired pulse ratios at various interstimulus intervals. Number of observations as in F.

(H) Working model for the roles of RIM C_2B at the active zone. C_2B targets RIM to PIP_2-containing membranes, recruiting its direct interaction partners and additional important fusion machinery to colocalize vesicle priming, Ca^{2+} influx and fusion with PIP_2. Many proteins that are important for release are activated by PIP_2 (highlighted in blue, with effect of PIP_2 indicated in *italic*). C_2B has an additional activity in synaptic vesicle release that may depend on PIP_2 at the active zone.

Author Manuscript Author Manuscript Author Manuscript Author Manuscript

All data shown as mean ± SEM, *p < 0.05, ** p < 0.01, *** p < 0.001 for IPSC and EPSC amplitude analyzed by one-way ANOVA (Kruskal Wallis; C,F), for PPRs analyzed by two-way ANOVA (D, G); all comparisons to cDKO. For analyses of rescue protein expression and example traces of PPRs, see Figure S7K–S7M.